

Kinetics and impacting factors of HO₂ uptake onto submicron atmospheric aerosols during a 2019 air quality study (AQUAS) in Yokohama, Japan

3 Jun Zhou^{a,b,c*}, Kei Sato^d, Yu Bai^e, Yukiko Fukusaki^f, Yuka Kousa^f, Sathiyamurthi Ramasamy^d,
4 Akinori Takami^d, Ayako Yoshino^d, Tomoki Nakayama^g, Yasuhiro Sadanaga^h, Yoshihiro
5 Nakashimaⁱ, Jiaru Li^c, Kentaro Murano^c, Nanase Kohno^c, Yosuke Sakamoto^{c,d,e}, Yoshizumi
6 Kajii^{c,d,e*}

⁷ ^aInstitute for Environmental and Climate Research, Jinan University, 511443 Guangzhou, China

⁸ ^bGuangdong-Hongkong-Macau Joint Laboratory of Collaborative Innovation for Environmental Quality,
⁹ Guangzhou 511443, China

10 ^aGraduate School of Global Environmental Studies, Kyoto University, Kyoto, 606-8501, Japan

11 ^dCenter for Regional Environmental Research, National Institute for Environmental Studies, Tsukuba, Ibaraki
12 305-8506, Japan

¹³Graduate School of Human and Environmental Studies, Kyoto University, Kyoto 606-8501, Japan

¹⁴Yokohama Environmental Science Research Institute, Yokohama Kanagawa 221-0024, Japan

15 ^aFaculty of Environmental Science and Graduate School of Fisheries and Environmental Sciences, Nagasaki
16 University, Nagasaki 852-8521, Japan

¹⁷ ^hGraduate School of Engineering, Osaka Prefecture University, Sakai, Osaka 599-8531, Japan

¹⁸ Graduate School of Agriculture, Tokyo University of Agriculture and Technology, 3-5-8 Saiwai-cho, Fuchu, Tokyo 183-8538, Japan

20 *Corresponding author.

Graduate School of Global Environmental Studies, Kyoto University, Kyoto 606-8501, Japan

E-mail address: kajii.yoshizumi.7e@kyoto-u.ac.jp and junzhou@jnu.edu.cn

25

26

28 Abstract

29 HO₂ uptake kinetics onto ambient aerosols play pivotal roles in tropospheric chemistry but are not fully
30 understood. Field measurements of aerosol chemical and physical properties should be linked to
31 molecular level kinetics; however, given that the HO₂ reactivity of ambient aerosols is low, traditional
32 analytical techniques are unable to achieve this goal. We developed an online approach to precisely
33 investigate the lower limit values of (i) the HO₂ reactivities of ambient gases and aerosols and (ii) HO₂
34 uptake coefficients onto ambient aerosols (γ) during 2019 air quality study (AQUAS) in Yokohama,
35 Japan. We identified the effects of individual chemical components of ambient aerosols on γ . The results
36 verified in laboratory studies on individual chemical components: transition metals play a key role in
37 HO₂ uptake processes and chemical components indirectly influence such processes (i.e., through
38 altering aerosol surface properties or providing active sites), with smaller particles tending to yield
39 higher γ values than larger particles owing to the limitation of gas phase diffusion is smaller with
40 micrometer particles and the distribution of depleting species such as transition metal ions is mostly
41 distributed in accumulation mode of aerosol. The modeling of γ utilized transition metal chemistry
42 derived by previous studies, further confirming our conclusion. However, owing to the high NO
43 concentrations in Yokohama, peroxy radical loss onto submicron aerosols has a negligible impact on O₃
44 production rate and sensitivity regime.

45 1 Introduction

46 As an important atmospheric trace gas, the hydroperoxyl radical (HO₂) links many of the key oxidants
47 in the troposphere, including the hydroxyl radical (OH), nitrate radical (NO₃⁻), ozone (O₃), and
48 hydrogen peroxide (H₂O₂) (Logan et al., 1981; Chen et al., 2001; Jaeglé et al., 2000; Sommariva et al.,
49 2004; Jacob, 2000). However, the observed HO₂ concentration in field measurements has not yet been
50 fully explained by sophisticated models (known as the “HO_x dilemma”) (Stone et al., 2012; Creasey
51 et al., 1997; Kanaya et al., 2007b; Whalley et al., 2010; Millán et al., 2015), although it can be mostly
52 solved in the conditions of clean marine air where NO concentration is low or aerosol loading is low

53 enough to make the heterogeneous reaction of HO₂ not important (Sommariva et al., 2004; Kanaya et
54 al., 2007a). Owing to the short atmospheric lifetime of HO_x(=OH+HO₂+RO₂), the HO_x reactivity
55 measurement can provide a robust test of its complex chemistry (Heard and Pilling, 2003). The HO₂
56 uptake kinetics onto ambient aerosols, including HO₂ reactivity (k_a) and uptake coefficient (γ), influence
57 many atmospheric processes, including ozone formation rate, ozone formation sensitivity to NO_x, and
58 H₂O₂ formation (Sakamoto et al., 2019; Thornton et al., 2008). With $\gamma > 0.1$, HO₂ concentration can
59 also be influenced under conditions such as low [NO] or high aerosol loading (Lakey et al., 2015; Mao
60 et al., 2013b; Martínez et al., 2003; Tie et al., 2001; Jacob, 2000; Matthews et al., 2014). These effects
61 make the HO₂ uptake onto ambient aerosols indirectly influence human health and climate change.

62 From laboratory, field, and modeling studies, HO₂ uptake coefficients onto different types of
63 aerosol can span several orders of magnitude (~0.002–1), which can be affected by many parameters,
64 such as droplet/particle size and composition, the presence of dissolved reactive gases, and
65 environmental conditions (i.e., relative humidity (RH), pH, and T) (Taketani et al., 2012; Taketani et al.,
66 2008; Bedjanian et al., 2005; Thornton et al., 2008; George et al., 2013; Lakey et al., 2016a; Lakey et
67 al., 2016b; Matthews et al., 2014; Cooper and Abbatt, 1996; Hanson et al., 1992; Thornton and Abbatt,
68 2005; González Palacios et al., 2016; Mozurkewich et al., 1987; Remorov et al., 2002; Jaeglé et al.,
69 2000; Loukhovitskaya et al., 2009; Stone et al., 2012). In the absence of metals, the uptake of HO₂ by
70 ambient aerosols is believed to occur *via* the acid–base dissociation of HO₂ (HO₂(g)
71 \leftrightarrow HO₂(aq); HO₂ \leftrightarrow O₂[−] + H⁺, $pK_a = 4.7$), followed by electron transfer from O₂[−] to HO₂(aq) (HO₂ +
72 O₂[−] $\xrightarrow{H_2O}$ H₂O₂ + O₂ + OH[−]), producing H₂O₂ (Jacob, 2000; Thornton et al., 2008; Zhou et al., 2019b).
73 However, laboratory studies have shown that certain transition metals (i.e., Cu(II) and Fe(II)) can act
74 as catalysts and accelerate HO₂ uptake rates onto many chemical compounds (Thornton et al., 2008;
75 Taketani et al., 2008; Taketani et al., 2012, Cooper and Abbatt, 1996). Owing to the sufficiently high
76 metal concentrations in tropospheric aerosols, as shown in previous field measurements (Hofmann et
77 al., 1991; Wilkinson et al., 1997; Guieu et al., 1997; Manoj et al., 2000; Halstead et al., 2000; Siefert et
78 al., 1998; Sedlak and Hoigné, 1993; Guo et al., 2014), recent studies have proposed that γ may be
79 dominated by metals contained in the aerosol. This can lead to the HO₂ destruction (Mao et al., 2013a;

80 George et al., 2013), forming H_2O_2 , HO_2 –water complexes, or water and sulfate (Mozurkewich et al.,
81 1987; Cooper and Abbatt, 1996; Gonzalez et al., 2010; Loukhovitskaya et al., 2009; Mao et al., 2010;
82 Macintyre and Evans, 2011), which are important in the evolution of the chemical composition and
83 physical properties of particles (George and Abbatt, 2010; George et al., 2008). The available data
84 concerning HO_2 uptake kinetics onto ambient aerosols are insufficient for quantitative consideration
85 owing to the much lower k_a value, as compared with the HO_2 reactivity of ambient gases (k_g). Therefore,
86 they are below the detection limits of the current instruments.

87 To our knowledge, aside from us, only one study has measured γ , using an offline method that
88 integrated ambient aerosols over size and time (Taketani et al., 2012). Considering that the offline
89 method may distort γ , we developed an online approach to evaluate HO_2 uptake kinetics onto ambient
90 aerosols. This method was successfully applied in Kyoto, Japan, in summer 2018, using a versatile
91 aerosol concentration enrichment system (VACES) and a technique combining laser-flash photolysis
92 with laser-induced fluorescence (LFP–LIF) (Zhou et al., 2019b). The obtained average γ value (~0.24)
93 was comparable with the previous values used for modeling studies (~0.2) (Stadtler et al., 2018; Jacob,
94 2000). However, the large standard deviation (± 0.20 , 1σ) of γ along with the measurement time suggest
95 that many other parameters might play a role, e.g., the measurement setup, aerosol characteristics, T ,
96 and RH.

97 In this study, we chose Yokohama (Japan), a coastal city with higher pollutant levels than Kyoto
98 and different properties of the air masses from mainland Japan and the coast, as the measurement site.
99 This is part of the Air QUAlity Study (AQUAS) campaigns. The chemical and physical properties of
100 ambient aerosols were quantified in real-time. To test their influence on k_a and γ , we conducted
101 correlation matrix analysis coupled with the bootstrap method and classified the arriving air masses
102 from different directions. Further, the main mechanism of γ was investigated by comparing the real-
103 time quantified γ values with the modeled values. The impact of the peroxy radical's loss onto ambient
104 aerosols on air quality is evaluated through their impact on ozone formation rates and their sensitivity
105 to NO_x . The results obtained here will for better estimation of the heterogeneous reaction between HO_2
106 and ambient aerosols in sophisticated air quality models.

107 **2 Materials and methods**

108 **2.1 Sampling sites**

109 The measurement campaign was conducted at Yokohama Environmental Science Research Institute in
110 Yokohama, Japan (location: 35°28'52.8"N, 139°39'30.3"E), from July 24 to August 03, 2019. The
111 sampling ports of the instruments were placed approximately 25 m above the ground. Figure S1 shows
112 the air mass directions during the campaign, which can be classified into two categories: (i) from the
113 sea to the north, toward Yokohama City (~19% of the experimental period: from 12:00 July 25 to 12:00
114 July 27, 2019) and (ii) from the mainland toward Yokohama City (~81% of the experimental period).
115 This classification was intended to distinguish the chemical properties of aerosols arriving from the
116 mainland and the ocean, and to consequently quantify their impacts on k_a and γ .

117 **2.2 Measurement strategies, instrumentation, and related data analysis**

118 **LFP–LIF** In situ ambient air HO₂ reactivity was measured using LFP–LIF, which was adapted from a
119 laser-induced pump and probe OH reactivity measurement technique. This approach has been
120 successfully employed for gas and aerosol phase HO_x (=OH+HO₂) reactivity measurements (Sadanaga
121 et al., 2004; Miyazaki et al., 2013; Sakamoto et al., 2018). Further details concerning the HO₂ reactivity
122 measurements are described in the Supporting Information (SI).

123 **VACES** To compensate for the relatively low ambient aerosol concentrations thus the low k_a , and the
124 low limit of detection (LOD) for the HO₂ reactivity measurement (~0.003 s⁻¹ with 240 decay
125 integrations), a setup with VACES and an auto-switching aerosol filter was used before LFP–LIF. The
126 VACES was built according to Sioutas et al. (1999), the ambient air sample was drawn into a tank
127 (containing ultra-pure water heated up to ~32 °C) of VACES through a PM_{2.5} cyclone at a flow rate of
128 over ~ 100 L min⁻¹, where the ambient air steam was saturated and subsequently cooled down in a
129 condenser connected above the tank (with a temperature of –2 °C). During this process, the water
130 droplets with diameters >2 µm formed on the collected ambient aerosols, which were then enriched by
131 a virtual impactor (with a 50% cutoff point less than 1 µm) and dried by passing through a diffusion
132 dryer connected right after the condenser in sequence. The concentration enrichment of the ambient

133 aerosols can be estimated using the total intake flow of VACES and the minor output flow of the virtual
134 impactor that connected to the aerosol instrumentations (more details are given in SI: the enrichment of
135 the ambient aerosols). Wang et al. (2013, 2014) claimed that when using the same technique as VACES
136 for the online measurement of copper in ambient aerosols, equivalent copper concentrations were
137 obtained compared to those measured by inductively coupled plasma mass spectrometer (ICP-MS) for
138 both total and water-soluble components, which indicates the impact of VACES system to the solubility
139 of Cu contained in ambient aerosol is negligible. Furthermore, previous studies found the liquid-liquid
140 phase separation RH ranged from 60%-100% in atmospherically relevant particles consisting of organic
141 species and inorganic salts (Yu et al., 2014), and the organic component appears to be the most useful
142 parameter for estimating the liquid-liquid phase separation, which was always observed for oxygen-to-
143 carbon elemental ratio ($O:C < 0.5$) and was never observed for $O:C \geq 0.8$ (Bertram et al., 2011). In this
144 study, the ambient aerosol $O:C$ ranged from 0.1 to 0.7, and the RH changing from ~80% (in ambient
145 air) to >100% (in water tank), and then to ~75% (in reaction cell), suggest that the phase separation may
146 have already happened before entering the VACES system, thus we assume the morphology of the
147 ambient aerosols didn't change during the concentration enrichment process. Unfortunately, we did not
148 measure the chemical composition after the VACES, thus we are not able to compare the chemical
149 composition of the post VACES aerosols to ambient aerosol. However, previous test using the ambient
150 aerosol fractions including coarse and fine PM indicated that the enrichment process of the VACES system
151 does not differentially affect the chemical composition of ambient PM (Kim et al., 2001), thus we assume
152 the chemical composition changing due to the enrichment process of the VACES can be neglected. The
153 enrichment factor of the ambient aerosol surface area (E) was calculated from the difference between
154 the surface areas measured before and after VACES by two scanning mobility particle sizers (SMPSs).

155 ***Aerosol physical properties and the enrichment factor of VACES*** The mass concentration and surface
156 area of ambient aerosols (before VACES) were determined using a Scanning Mobility Particle Sizer
157 (SMPS₁, model 3936L72, TSI, measure particle size distribution at 14.1–736.5 nm, 5-min intervals).
158 The mass concentration of PM_{2.5} was measured using a palm-sized optical PM_{2.5} sensor (Nakayama et
159 al., 2018). In order to test the enrichment factor of the VACES, a SMPS₂ (model 3936L75, TSI, measure
160 particle size distribution at 14.6–661.2 nm, 5-min intervals) was used to measure the enriched mass

161 concentration and surface area of ambient aerosols (after VACES) for ~ 2 hours every day for ~ 6 days.
 162 The enrichment factor of VACES for the surface area was estimated as 12.5 ± 2.5 from the ratio
 163 between S_2 and S_1 , where S_2 and S_1 are the averaged surface areas measured by SMPS₂ and SMPS₁ of
 164 each day, respectively. According to the test from previous study of the VACES system, there is no
 165 distortion of the size distribution of the original ultrafine aerosols as the particle concentration
 166 enrichment occurs without any coagulation (Sioutas et al., 1999), here we listed the mean radius and
 167 geometric standard deviation (Geo. Std. Dev.) of the ambient aerosols before and after VACES during
 168 the enrichment factor measurement periods, as shown in Table 1. We could see that the mean radius
 169 before and after VACES are not statistically different within the standard deviation.

170 **Table 1:** The Mean radius and Geometric standard deviation of ambient aerosols before and after VACES

Experimental time*	Before VACES		After VACES	
	Mean radius (nm)	Geo. Std. Dev.	Mean radius (nm)	Geo. Std. Dev.
2019.7.25 09:03 – 11:03	129.47 \pm 11.32	0.92 \pm 0.04	133.19 \pm 3.37	0.92 \pm 0.02
2019.7.26 09:30 – 11:30	94.95 \pm 14.42	0.99 \pm 0.09	85.09 \pm 14.96	1.01 \pm 0.09
2019.7.27 10:00 – 12:00	85.09 \pm 14.96	1.01 \pm 0.09	80.40 \pm 21.01	1.01 \pm 0.07
2019.7.28 09:30 – 11:30	163.62 \pm 13.32	1.01 \pm 0.08	164.06 \pm 14.40	1.04 \pm 0.06
2019.7.29 09:10 – 11:10	128.06 \pm 6.90	0.91 \pm 0.02	125.07 \pm 7.68	0.92 \pm 0.02
2019.7.30 09:30 – 11:30	111.40 \pm 8.21	1.01 \pm 0.02	115.32 \pm 6.26	1.01 \pm 0.03

171 *represent the time period of the enrichment factor measurements;

172 \pm represent the standard deviation of the averaged values of mean radius and Geo. Std. Dev.

173 The enriched surface area of ambient aerosols with aerodynamic diameter $< 0.74 \mu\text{m}$ (PM_{0.74}) was
 174 calculated from the surface area of ambient aerosol measured by SMPS₁ and the enrichment factor. The
 175 enriched surface area of PM_{2.5} was then calculated by multiplying the enriched surface area of PM_{0.74}
 176 by the mass ratio between PM_{2.5} and PM_{0.75} (~ 1.1), where we assume the surface area are increased in
 177 proportional to the mass concentration. However, as the larger particles (here referred to particles ranged
 178 from 0.74 to 2.5 μm) tend to have lower surface area than the smaller particles, we consider the obtained
 179 enriched surface area of PM_{2.5} as the upper limit value. More details can be found in SI.

180 **HO₂ uptake kinetics** After passing through the VACES system, the ambient air was sampled using a
 181 three-port valve (Bolt, Flon Industry Co., LTD) and injected into the LFP–LIF system. The valve was
 182 switched automatically between two sampling lines, one with the aerosol filter on, and the other one

183 with the aerosol filter off, HO₂ reactivities in ambient air caused by two modes were measured: (a) the
184 gas phase mode with aerosol filter on, the HO₂ reactivities are represented as k_g , and (b) the gas +
185 enriched aerosol phase mode with aerosol filter off, the HO₂ reactivities are represented as $k_g + Ek_a$, where
186 E represents the enrichment factor of k_a , Ek_a represents the total HO₂ reactivities caused by enriched
187 ambient aerosols, the usage of Ek_a is based on the assumption that HO₂ uptake with aerosol particles
188 follows the pseudo-first-order rate law. We modeled k_g in both modes using a theory identified
189 previously (see SI: HO₂ reactivity of ambient gas phase) (Zhou et al., 2019b) and compared it with the
190 measured values. The differences between measured and modeled k_g in mode (a) enabled us to establish
191 their interrelationship and to check instrument stability. The differences between $(k_g + Ek_a)$ and the
192 modeled k_g in mode (b) are considered as the enriched aerosol phase HO₂ reactivity (Ek_a). The total HO₂
193 reactivity decay profile follows single-exponential decay:

194
$$HO_2 = [HO_2]_0 \exp(-(k_g + Ek_a + k_{bg})t) \quad (1)$$

195 where k_{bg} denotes the zero air background obtained by injecting zero air with the same RH as the real-
196 time ambient value into the reaction cell every 24 h for 30 min. The RH was controlled by passing some
197 of the zero air through a water bubbler. The value of k_{bg} was subtracted separately on each day. The
198 variability of k_{bg} (i.e., the reproducibility of the laser system) was calculated as the standard deviation
199 of the response of repeated measurements on different days. It was found to be ~4%, which is slightly
200 higher than the instrument precision (3%). A 30-min average calculation was applied to the data to
201 reduce data fluctuation. The observed HO₂ uptake coefficients onto ambient aerosols (γ_{obs}) can be
202 calculated from the dependence of Ek_a on γ_{obs} :

203
$$Ek_a = \frac{\gamma_{obs} \omega_{HO_2} ES}{4} \quad (2)$$

204 where ES and ω_{HO_2} represent the enriched surface area of ambient aerosol after VACES and the mean
205 thermal velocity of HO₂ (~437.4 m s⁻¹), respectively. The uncertainty of the enriched surface area was
206 estimated from the instrument systematic error of SMPS (~ 8%) and the uncertainty of the enrichment
207 factor (± 2.5), which are shown in Fig.1b (see SI). The HO₂ reactivity of ambient aerosol (k_a) can be
208 obtained from Ek_a by dividing by the enrichment factor E .

209 **High resolution–time of flight–aerosol mass spectrometry (HR–ToF–AMS)** A field-deployable HR–
210 ToF–AMS (Aerodyne Research Inc.) (DeCarlo et al., 2006) was used for the characterization of the
211 non-refractory aerosol mass with a time resolution of ~3 min. The HR-ToF-AMS measured the total
212 organic aerosol (OA), sulfate (SO_4^{2-}), nitrate (NO_3^-), ammonium (NH_4^+), chloride (Cl^-), and the two
213 most dominant oxygen-containing ions in the OA spectra, i.e., mass-to-charge ratios of $m/z = 44$ (Org44,
214 mostly CO_2^+) and $m/z = 43$ (Org43, mainly $\text{C}_2\text{H}_3\text{O}^+$ for the oxygenated OA and C_3H_7^+ for the
215 hydrocarbon-like OA) (Ng et al., 2011). The fractions of Org44 and Org43 in OA are represented as f_{44}
216 and f_{43} , respectively. Ambient air was sampled through a critical orifice into an aerodynamic lens, which
217 efficiently transmitted particles between 80 nm and up to at least 1 μm . Particles were flash-vaporized
218 by impaction on a resistively heated surface (~600 °C) and ionized by electron ionization (70 eV). The
219 m/z values of the resulting fragments were determined using a ToF mass spectrometer. Data were
220 analyzed using the ToF–AMS software SQUIRREL and PIKA. Data were not corrected for lens
221 transmission efficiency. Standard relative ionization efficiencies (RIE) were used for organics (RIE =
222 1.4), nitrate (RIE = 1.1), chloride (RIE = 1.3), sulfate (RIE = 1.12), and ammonium (RIE = 4).
223 Concentration data were obtained from background-subtracted stick-mass data (low-mass-resolution-
224 base mass concentration data, which are calibrated using ammonium sulfate particles) and determined
225 assuming a collection efficiency (CE) of 0.5.

226 **Filter-based photometer** Real-time measurement of the equivalent black carbon (eBC) was performed
227 using a 5-wavelength dual-spot absorption photometer (MA300, AethLabs, San Francisco, CA, USA),
228 which performed an online correction for possible artefacts resulting from filter loading and multiple
229 scattering (Drinovec et al., 2015). In this study, eBC data obtained from light attenuation at a wavelength
230 of 880 nm were used to avoid possible contributions from brown carbon; the time resolution was ~1
231 min.

232 **Trace elements** Fourteen trace elements (Al, V, Cr, Mn, Co, Ni, Cu, Zn, As, Se, Sr, Cd, Ba, and Pb)
233 were measured using an offline method at two-day intervals from 21 July to 5 August 2019. The
234 suspended particulate matter (SPM) was collected onto 623.7 cm^2 size quartz fiber filters (Pallflex
235 Tissuquartz 2500QAT-UP), which had an available collecting area of 405.84 cm^2 , using a high-volume

236 sampler (1000 L min⁻¹). Approximately 2 cm² of each filter was cut into pieces and placed into a
237 polytetrafluoroethylene (PTFE) pressure digestion tank with 1 mL 49% hydrofluoric acid (HF) and 5
238 mL 69% nitric acid (HNO₃). A Thermo Fisher X2 Series ICP–MS was then used to determine metal
239 concentrations. By assuming that the metal fractions were the same in SPM and PM₁ (aerosol
240 particles with aero-dynamic diameters less than 1 μm), the concentrations in PM₁ were estimated
241 according to the tested metal concentrations in SPM and the ratio between SPM and PM₁ measured in-
242 situ.

243 **Water-soluble inorganic species** NR-PM₁ water-soluble inorganic species (including Na⁺, SO₄²⁻, NH₄⁺,
244 NO₃⁻, Cl⁻, Ca²⁺, K⁺, Mg²⁺) used for the *ISORROPIA-II model* were also measured using offline method,
245 as described above. For extraction, we cut 1/4 of a 47 mm filter punched from the original collected
246 filter and placed it in 10 mL of ultrapure water (18.2 MW cm⁻¹) in a centrifuge tube. This was followed
247 by 15 min of ultrasonication in a 30°C water bath. The solution was then vortexed (Vortex Genie 2,
248 Scientific Industries, USA) for 1 min to ensure homogeneity and filtered through syringe filter with
249 pore size of 0.45- μm (Advantec Dismic-25, PTFE). An Ion Chromatograph (IC, ICS1600, DIONEX,
250 USA) was employed to determine the concentrations of these inorganic ions in the extracted solution.

251 **Gas phase monitors** NO₂ was measured by cavity attenuated phase shift (CAPS, Aerodyne Research,
252 USA, at 1-s intervals), NOy—NO by chemiluminescence (Model 42i-TL, Thermo, at 10-s intervals),
253 CO by Thermo CO analyzer of nondispersive infrared spectroscopy (Model 48i-TLE, Thermo Scientific,
254 USA, at 10-s time intervals), and O₃ by UV absorption (Model 1150, Dylec, AMI Co., Ltd, at 10-s time
255 intervals). HCHO was determined by high performance liquid chromatography (HPLC; 1260 Infinity,
256 Agilent Technologies Inc, USA) from 14:00 July 29, to 12:00 August 3, 2019. An average value of ~2
257 ppb was used for the data analysis.

258 **ISORROPIA-II model** NR-PM₁ water-soluble inorganic species (including Na⁺, SO₄²⁻, NH₄⁺, NO₃⁻, Cl⁻,
259 Ca²⁺, K⁺, Mg²⁺) and meteorological parameters including temperature and RH were used to calculate
260 the aerosol pH and liquid water content based on the *ISORROPIA-II* model (Fountoukis and Nenes,
261 2007). We ran *ISORROPIA-II* in “reverse” mode and the particles were assumed to be deliquescent, i.e.,

262 in metastable mode (Hennigan et al., 2015). The thermodynamic equilibrium of the $\text{NH}_4^+ - \text{SO}_4^{2-} - \text{NO}_3^-$ system case was used for modeling.

264 3 Results and discussion

265 3.1 The HO_2 uptake kinetics onto ambient aerosols

266 The measured total HO_2 reactivities were compared against the modeled gas phase HO_2 reactivity under
267 the experimental conditions both with and without the aerosol phase. Without the aerosol phase, the
268 modeled k_g values are calculated according to the description in Sect. 2.2, which are not statistically
269 different with the measured k_g values (Fig. 1a second panel, T-test, $p = 0.49$, with inspection level =
270 0.05), indicating that HO_2 loss in the reaction cell was dominated by its reaction with NO_2 in the LFP-
271 LIF system. With the aerosol phase, the measured ($Ek_a + k_g$) and modeled values ($\approx k_g$) were significantly
272 different (see Fig. 2b, first panel, T-test, $p = 0.04$, with inspection level = 0.05). The differences were
273 considered to be the HO_2 reactivities of enriched ambient aerosols (Ek_a). Ek_a ranged between 0.015 s^{-1}
274 (25^{th} percentile) and 0.097 s^{-1} (75^{th} percentile), with the median value of 0.059 s^{-1} , the corresponding k_a ,
275 calculated by dividing Ek_a by E , ranged between 0.001 s^{-1} (25^{th} percentile) and 0.008 s^{-1} (75^{th} percentile),
276 with the median value of 0.005 s^{-1} and average value of $0.005 \pm 0.005 \text{ s}^{-1}$. The error for Ek_a was estimated
277 as $\sim 0.05 \text{ s}^{-1}$, calculated as the propagated error from $k_g + Ek_a$ (i.e., the systematic error of the instrument,
278 $\sim 0.05 \text{ s}^{-1}$) and the modeled k_g in mode (b) ($\sim 0.001 \text{ s}^{-1}$). The error for k_a was then estimated as ~ 0.004
279 s^{-1} by dividing the error of Ek_a by the enrichment factor E . The corresponding γ , calculated from Eq.
280 2, ranged from 0.05 (25^{th} percentile) to 0.33 (75^{th} percentile), with the median value of 0.19 (with an
281 average value of 0.23 ± 0.21). The mean diameter of ambient particles ranged from 0.1 to $0.46 \mu\text{m}$ (with
282 the median value of $0.25 \mu\text{m}$), the gas-phase diffusion effects on γ were estimated to be $\sim 6.6 \%$ (further
283 details are given in the SI). The absolute increase of γ due to the gas-phase diffusion is 0.03 on average,
284 which is negligible compared to γ uncertainty (~ 0.21 on average). Therefore, we ignored the gas-phase
285 diffusion effects to γ .

286

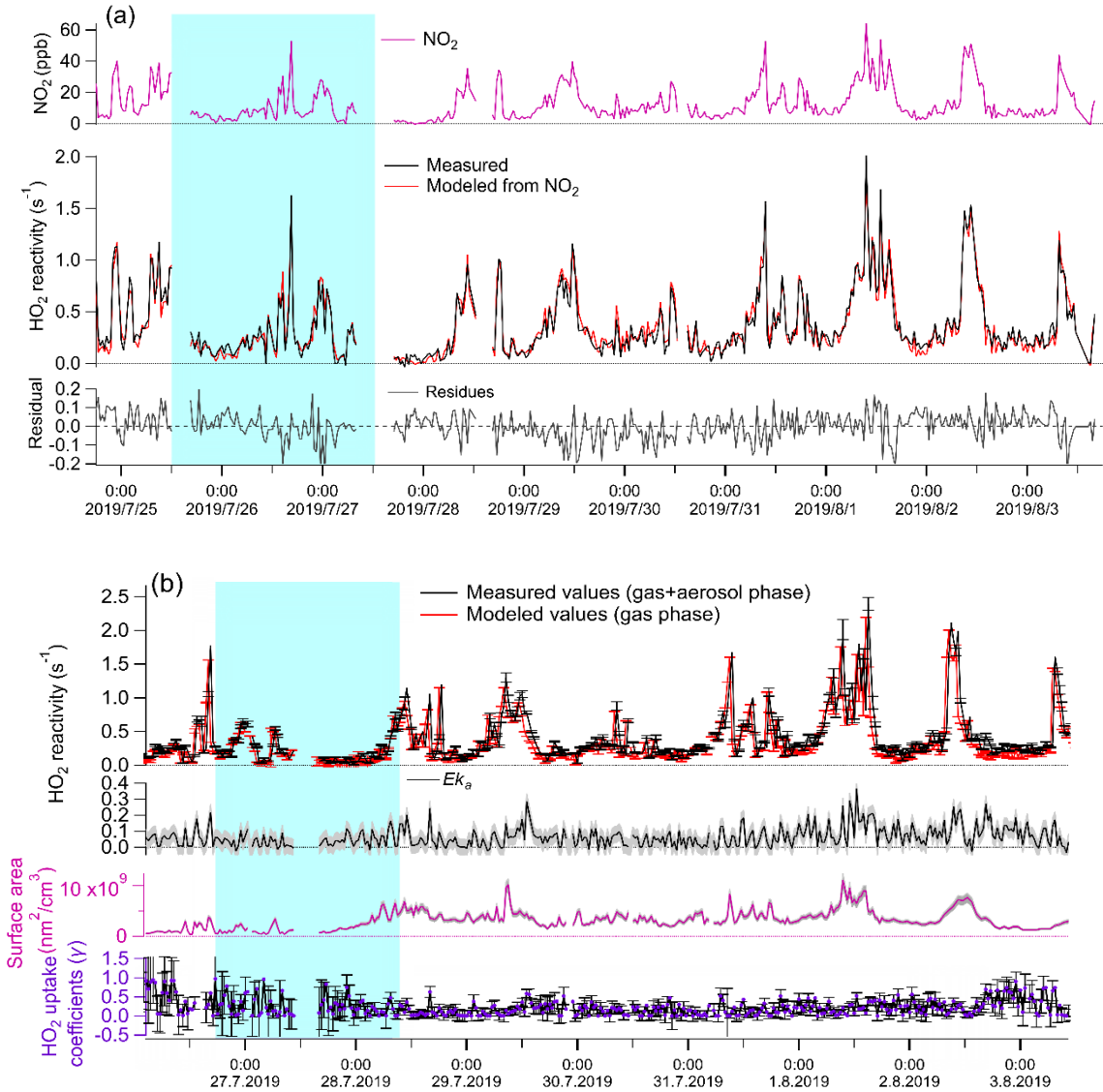
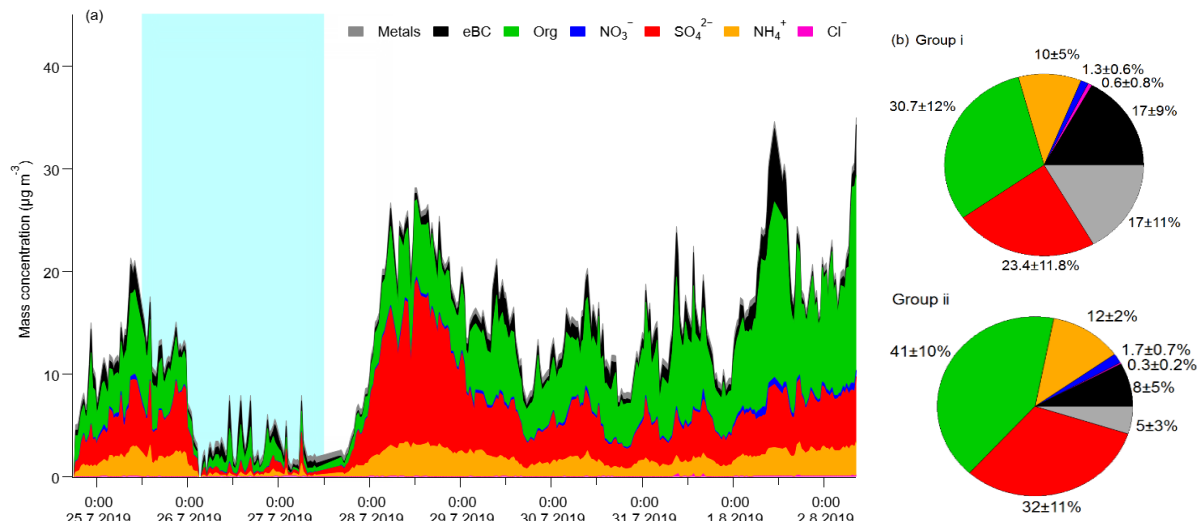


Figure 1: Temporal variation of parameters under different experimental conditions. (a) Without aerosol phase: 1st panel: measured NO_2 concentrations (ppb); 2nd panel: measured (red line) and modeled (black line) k_g ; 3rd panel: fitting residues of modeled k_g values, ranging from -0.04 (25 percentile) to 0.05 (75 percentile), therefore we consider the systematic error of the LFP-LIF instrument to be $\sim 0.05 \text{ s}^{-1}$. (b) Gas + aerosol phase: 1st panel: measured total HO_2 reactivity ($k_g + Ek_a$) and modeled k_g ; 2nd panel: Ek_a calculated from the difference between the measured and modeled values from the 1st panel, the gray shadow area represents the uncertainty of Ek_a (ΔEk_a), propagated from the error of ($k_g + Ek_a$) and modeled k_g ; 3rd panel: the upper limit surface area of the enriched ambient aerosols (ES), the gray shadow area represents the uncertainty of ES (ΔES), propagated from the systematic errors of the SMPS instrument ($\sim 8\%$), and the uncertainty of the enrichment factor; 4th panel: γ calculated from Ek_a and ES according to Eq. 2. The errors for γ were propagated from ΔEk_a and ΔES , $\Delta \gamma = \gamma \times \sqrt{\frac{\Delta Ek_a^2}{Ek_a} + \frac{\Delta ES^2}{ES}}$. The blue shaded area represents the air masses from group i (from coast), the remainder is from group ii (from mainland).

Statistical significance analysis showed that the average γ value of group i (0.35 ± 0.28) is significantly higher than that of group ii (0.21 ± 0.16) (calculated $p = 4.9\text{E-}5$; Mann-Whitney), indicating that the air masses from the ocean yield higher γ values than the air masses from mainland Japan. The difference in γ values between group i and group ii may due to the different chemical

328 components contained in the ambient aerosols arrived from the ocean or mainland, which we will
 329 discuss in the following sections. The average value of k_a at Yokohama ($0.005 \pm 0.005 \text{ s}^{-1}$) was much
 330 higher than that at Kyoto city ($0.0017 \pm 0.0015 \text{ s}^{-1}$) (with calculated $p < 0.05$; Mann-Whitney), this may
 331 due to the different aerosol properties in Kyoto and Yokohama city. We list some of them as follows:
 332 1) mass composition, the aerosols at the coast city (Yokohama) tend to contain more sea salts thus
 333 increased k_a , 2) particle size distribution, smaller particles tend to yield higher γ values than larger
 334 particles owing to the depleting species (e.g., transition metal ions) are mostly distributed in
 335 accumulation mode of aerosol, 3) the water content and the metal concentrations, which will highly
 336 influence the HO_2 uptake capacity of the ambient aerosols. However, the average value of HO_2 uptake
 337 coefficient onto ambient aerosols (γ) at Yokohama is ~ 0.23 , which is comparable with previous
 338 measured (~ 0.24 – 0.25) (Zhou et al., 2019b; Taketani et al., 2012) and modeled (~ 0.20) values (Stadtler
 339 et al., 2018; Jacob, 2000). The large standard deviation (± 0.21 , 1σ) of the values along with the
 340 measurement time may be due to the instantaneously changed chemical and physical properties of
 341 ambient aerosols, indicating that a large bias may exist if a constant γ value is used for modeling.

342 3.2 Bulk chemical composition of ambient aerosols



343
 344 Figure 2: (a) Concentrations of non-refractory chemical components plus eBC in Yokohama, Japan (July 24 to
 345 August 02, 2019). The blue shaded area represents group i from coast and the remaining areas represent group ii
 346 from mainland. (b) Average contribution fractions of different chemical components of groups i and ii.
 347
 348 Figure 2a shows the time series of the mass concentrations of OA, SO_4^{2-} , NO_3^- , NH_4^+ , Cl^- , and eBC in
 349 PM_1 in Yokohama from July 24 to August 02, 2019, which is ~ 1.5 days less than for the LFP–LIF data.

350 During this period, PM_1 ranged from ~ 1 to $35 \mu g m^{-3}$ (average $\approx 13 \mu g m^{-3}$) and was dominated by OA,
351 SO_4^{2-} , and NH_4^+ , with contributions of $39 \pm 11\%$, $30 \pm 12\%$, and $12 \pm 4\%$, respectively; these were
352 followed by eBC and metals, with contributions of $10 \pm 7\%$ and $8 \pm 8\%$, respectively. Cl^- contributed
353 $< 1\%$ in both groups, which is similar to that reported for an urban area in winter in Bern (Switzerland)
354 (Zhou et al., 2019a). However, NO_3^- contributed much less ($\sim 2 \pm 0.7\%$) compared with that reported
355 for Bern ($\sim 19 \pm 4\%$), which may be due to the reverse reaction of NH_4NO_3 converting to HNO_3 . Since
356 Yokohama is a coastal city, and HNO_3 is easily vaporized in summer, gaseous HNO_3 may sink with sea
357 salt particles by forming $NaNO_3$ through heterogeneous reactions (Finlayson-Pitts and Pitts, 2000).

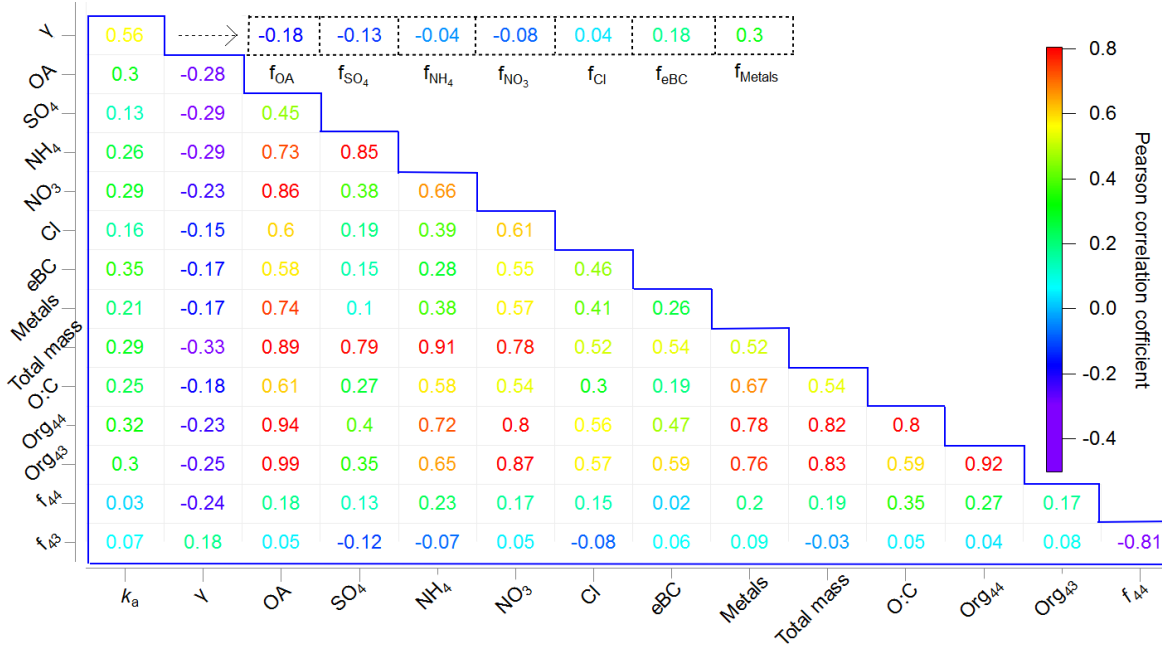
358 Figure 2b shows the average contribution fractions of different components of group i and group
359 ii. The main differences in the components between these two groups are the fractions of OA, BC, SO_4^{2-} ,
360 and metals. The OA fraction was ~ 1.8 and ~ 8.4 times higher than that for the metals in groups i and ii,
361 respectively. As OA can cover the surface of the particles and thereby decrease γ (Lakey et al., 2016a;
362 Takami et al., 2013), the difference between the OA and metal fractions in these two groups may
363 partially explain the much higher γ values of group i (vs. group ii). Previous studies have shown quite
364 low HO_2 uptake coefficient on BC (~ 0.01) (Saathoff et al., 2001; Macintyre and Evans, 2011), which
365 is different with the result obtained here. This may be due to the much higher fraction of BC in group i
366 (vs. group ii) provide active sites for HO_2 self-reaction or its reaction with the H atom from the
367 abstraction reaction from hydrogen containing functional groups and form H_2O_2 (Bedjanian et al., 2005),
368 or BC can be coated with additional materials (e.g., sulfate and organic carbon) thus influence HO_2
369 uptake (Schwarz et al., 2008). We also observed slightly higher Cl^- and BC fraction in group i (from
370 ocean) than that in group ii (from mainland), which may be due to the effects of sea salt and the ship
371 emissions in the air mass from the ocean, respectively. From the average diurnal patterns (Figs. S5 and
372 S6), the trends in k_a follow the trends in chemical composition, whereas γ shows a contrasting trend
373 with both variables in both groups. For group ii, SO_4^{2-} and OA exhibited higher values whereas γ
374 exhibited lower values during the daytime than those during nighttime, indicating that secondary aerosol
375 formation resulting from photochemical reactions may decrease γ . To identify the influence of each

376 individual chemical component of ambient aerosol on k_a and γ , we further performed correlation matrix
377 analysis.

378 **3.3 Influence of individual chemical components of ambient aerosol on k_a and γ**

379 For multiple-component ambient aerosol, k_a and γ are influenced by different chemical components,
380 these chemical components may also have mutual effects to each other, for example, the transition metal
381 Cu and Fe contained in ambient aerosols can be chelated by organics (Lakey et al., 2016b). Therefore,
382 we produced a Pearson correlation matrix of all the testing factors at Yokohama city, including different
383 chemical components, k_a and γ . Here we note that the different chemical components were measured
384 using HR–ToF–AMS for ambient aerosols with aerodynamic diameters $< 1 \mu\text{m}$, while k_a and γ were
385 measured using VACES–LFP–LIF system for ambient aerosols with aerodynamic diameters $< 2.5 \mu\text{m}$,
386 but due to most “fine-mode” aerosols have the mean diameter ranged from $0.09 \mu\text{m}$ to $0.47 \mu\text{m}$ (with
387 the median value of $0.25 \mu\text{m}$, measured by SMPS), we assume the chemical components of ambient
388 aerosols with the aerodynamic diameter ranged between $1 \mu\text{m}$ and $2.5 \mu\text{m}$ have negligible impact on
389 Pearson correlation matrix result. However, present results do not include the effects of coarse particles
390 (with aerodynamic diameters $> 2.5 \mu\text{m}$) to the HO_2 uptake kinetics, and we may partially miss
391 measuring sea spray (with diameters ranged from ~ 0.05 to $10 \mu\text{m}$) effects. When Cl^- measured by
392 AMS increased, coarse particles may exist and our results may not represent the real ambient
393 conditions. Consequently, we consider our results as the lower limit of the HO_2 uptake kinetics onto
394 real ambient aerosols.

395 To exclude the effects of the different fractions of chemical components in groups i and ii, the
396 bootstrap method, which is based on the creation of replicate the inputs by perturbing the original data
397 through resampling, was employed. The resampling was performed by randomly reorganizing the rows
398 of the original time series such that some rows of the original data were present several times while
399 other rows were removed. The final results were obtained by running the data for 1000 bootstrap
400 replicates. The average values of these 1000 bootstrap replicates are listed in Fig. 3.



401

402 Figure 3: Correlation matrix showing Pearson's r values for the chemical compositions, k_a , and γ during the
 403 corresponding measurement periods (in the blue box), as well as the Pearson's r values for the chemical
 404 composition fraction i (represented as f_i , $i = OA, SO_4^{2-}, NH_4^+, NO_3^-, Cl^-, eBC$, and metals) and γ (in the dashed
 405 line box).

406

407 Most of the chemical components had strong or moderate Pearson correlation coefficients with each
 408 other (Fig. 3), although k_a and γ showed only a moderate correlation with each other (0.56). As γ can be
 409 correlated with the qualitative, rather than quantitative, properties of the aerosols, we further
 410 investigated the Pearson's r values between the chemical composition fractions and γ . The results show
 411 that k_a was positively correlated with total mass and the individual chemical components, whereas γ
 412 showed only a weak positive correlation with f_{Metals} (0.30) and f_{eBC} (0.18). According to previous
 413 studies, metals may act as a catalyst thus accelerating the depletion of HO_2 (Mao et al., 2013a), and BC
 414 can provide active sites or can be coated by other chemical components thus facilitating the HO_2 uptake
 415 (Bedjanian et al., 2005; Schwarz et al. (2008), as described in Sect.3.2. The very weak correlation of γ
 416 with f_{Cl^-} (0.04) may be related to Cl^- chemistry, for example, $HO_2(g)$ can react with $NaCl(g)$, produce
 417 $NaOH$ and $Cl_2(g)$, thus cause a decrease in the HO_2 concentration and indirectly effects γ (Remorov et
 418 al., 2002). Interestingly, when considering the Org44 and Org43 fractions in total OA separately, γ is
 419 positively correlated with f_{43} (0.18) but negatively correlated with f_{44} (-0.24). This is consistent with
 420 previous conclusion that more oxidized organic aerosols tend to be highly viscous and thus decrease
 421 HO_2 uptake coefficients (Lakey et al., 2016b). In summary, γ was dominated by the free forms of

422 transition metals that can act as catalysts of HO₂ uptake onto ambient aerosols, and was indirectly
 423 affected by chemical components that might alter the properties of ambient aerosols, e.g., oxygenated
 424 OA can cover the aerosol surface and alter the viscosity of ambient aerosols, thereby decrease γ (Lakey
 425 et al., 2016a; Lakey et al., 2016b; Takami et al., 2013), whereas BC may provide active sites or be
 426 coated by other chemical components, thereby increase γ . This is further confirmed by the classification
 427 of the air masses, i.e., the air mass from the ocean (group i), which contained less OA and more metals
 428 than that from mainland Japan (group ii), had a higher HO₂ uptake capacity. We further compared the
 429 measured γ values with the modeled γ values using previously proposed mechanisms, as shown below.

430 **3.4 Possible mechanism of HO₂ uptake onto ambient aerosols**

431 Two mechanisms of HO₂ uptake onto aqueous ambient aerosols have been proposed, for which
 432 equations have been derived from a previous study (Thornton et al., 2008): (i) HO₂-only chemistry and
 433 (ii) chemistry with transition metals playing a role. In this study, the liquid content of the total ambient
 434 aerosol mass ranged from 70% to 88%, as obtained from the *ISORROPIA-II model*. As the solubility of
 435 Fe is rather small in ambient aerosol, the reaction rates of Fe/Mn for liquid phase HO₂ in aerosol is ~
 436 100 times slower than it is for Cu, thus the influence of Fe and Mn on HO₂ uptake can be neglected
 437 compared to Cu or scaled as equivalent [Cu²⁺] (Fang et al., 2017; Hsu et al., 2010; Baker and Jickells,
 438 2006; Oakes et al., 2012; Song et al., 2020), therefore, we use the soluble Cu as surrogate for transition
 439 metals in ambient aerosols to assess their influence to γ . The Cu solute mass fraction in the liquid content
 440 of the ambient aerosols was estimated as $(3.5\text{--}30) \times 10^{-4}$ mol L⁻¹ according to our offline filter test
 441 (Sect. 2.2), and to get the effective concentrations of Cu ions which can participate in the reaction of
 442 the destruction of peroxy radicals, the activity coefficient for total Cu was assumed to be 0.1 (upper
 443 limit) based on a study of (NH₄)₂SO₄ particles at 68% RH (Ross and Noone, 1991; Robinson and Stokes,
 444 1970). Using copper ions as a surrogate metal for transition metal ions (TMIs), the potential HO₂ loss
 445 onto aqueous ambient aerosols via mechanisms involving TMIs was estimated as (Hanson et al., 1994):

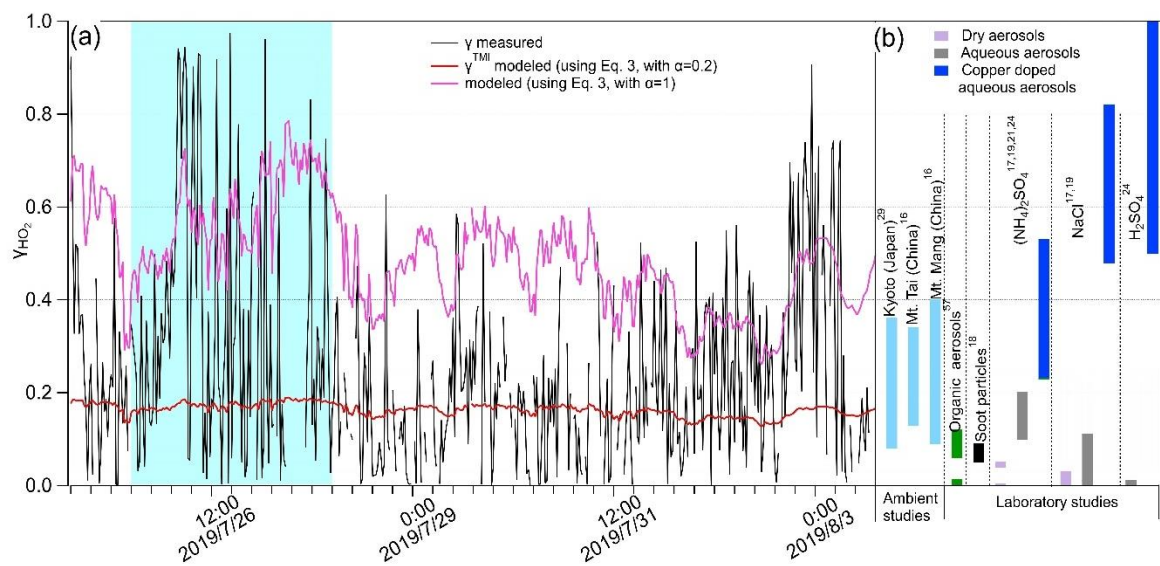
$$446 \frac{1}{\gamma^{\text{TMI}}} = \frac{1}{\alpha^{\text{HO}_2}} + \frac{\omega}{H_{\text{eff}}RT \sqrt{k^I D_{\text{aq}} Q'}} \quad (3)$$

447 where α^{HO_2} is the mass accommodation coefficient of HO_2 , ω is the mean HO_2 molecular speed (cm
 448 s^{-1}), H_{eff} is the effective Henry's Law coefficient, R is the gas constant ($\text{J K}^{-1} \text{ mol}^{-1}$), and T the
 449 temperature (K). k^{I} is the pseudo-first-order rate constant equal to $k_{\text{TMI}}^{\text{II}}[\text{TMI}]$, where $k_{\text{TMI}}^{\text{II}}$ is the second
 450 order rate constant for aqueous phase reaction with HO_2/O_2^- and TMI. Q' accounts for aqueous-phase
 451 diffusion limitations and is expressed as

$$452 \quad Q' = [\coth(q) - \frac{1}{q}]; q = r_p \sqrt{\frac{k^{\text{I}}}{D_{aq}}} \quad (4)$$

453 Table S1 shows more details of the parameters used for modeling. Previous laboratory studies suggest
 454 the mass accommodation coefficient for various single-component aerosols doped with Cu(II) is
 455 commonly > 0.2 (Taketani et al., 2008, 2009; Mozurkewich et al., 1987; Thornton and Abbatt, 2005;
 456 George et al., 2013; Lakey et al., 2016a, 2016b), and organics substantially reduce HO_2 uptake onto
 457 aerosols containing TMI (Lakey et al., 2016b). Here we calculated γ^{TMI} with $\alpha^{\text{HO}_2}=0.2$ using Eq. 3,
 458 which are plotted in Fig. 4a along with the measured γ values; the much lower variation of the modeled
 459 values may due to the low time resolution (~ 2 days) of $[\text{Cu}]$. The measured γ values (~ 0.23 on average)
 460 are significantly higher than the modeled γ^{TMI} with $\alpha^{\text{HO}_2}=0.2$ (~ 0.16 on average), with calculated
 461 $p<0.05$ (t-test), which may due to the TMI contained in the ambient aerosol. However, when using the
 462 upper limit of the mass accommodation value for modelling (with $\alpha^{\text{HO}_2}=1$), the measured γ values are
 463 significantly lower than the modelled γ^{TMI} (averaged value: ~ 0.50), these results indicating that the
 464 chemical components may be internally mixed, as proposed by Takami et al. (2013), which influences
 465 the aerosol surface tension and the activity of the free form of the copper ion (i.e., OA and BC) to
 466 constrain γ^{TMI} . We suggest that the additional collective effects of different chemical components to
 467 α^{HO_2} and the bulk reactions should be involved in the γ^{TMI} modelling to get accurate estimation. No
 468 linear correlation was found between γ^{TMI} and γ . Further classification of measured $\gamma \geq 0.4$ and $\gamma < 0.4$
 469 shows that γ^{TMI} has a weak correlation with measured γ values when $\gamma \geq 0.4$ (Fig. S7), which may due
 470 to the higher fraction of metals in the total mass at measured $\gamma \geq 0.4$ ($\sim 12\%$) than at < 0.4 ($\sim 7\%$);
 471 therefore, the impact of the other chemical components is much lower. The γ values obtained here are
 472 comparable with those in previous ambient aerosol studies (Taketani et al., 2008; Zhou et al., 2019b) (Fig.

473 5b). When compare with single-compound aerosols obtained from laboratory studies, γ values were
 474 generally higher than the HO₂ uptake coefficients onto organic species (Lakey et al., 2015), soot particles
 475 (Bedjanian et al., 2005), and the dry state of inorganic aerosols (i.e., (NH₄)₂SO₄, NaCl, and H₂SO₄), but
 476 comparable or lower than aqueous and copper-doped aqueous phases of inorganic species (Fig. 4b) (George
 477 et al., 2013; Lakey et al., 2016b; Taketani et al., 2008; Thornton and Abbatt, 2005). This may indicate the
 478 collective effects of the individual chemical components of ambient aerosols to γ , and the significant
 479 influence of RH to aerosol states of single-component particles thus their HO₂ uptake coefficients.



480
 481 Figure 4: (a) Measured and modeled γ values along with measurement time. The blue shaded area represents group
 482 i; the remaining areas represent group ii. (b) HO₂ uptake coefficients onto different types of aerosol obtained from
 483 ambient and laboratory studies, the numbers indicate the related references from which the data were obtained: 1.
 484 Zhou et al., 2019b; 2. Taketani et al., 2012; 3. Lakey et al, 2015; 4. Bedjanian et al., 2005; 5. Taketani et al., 2008;
 485 6. George et al., 2013; 7. Lakey et al., 2016b; 8. Thornton and Abbatt, 2005.

486
 487 Other studies have shown that γ is strongly negatively temperature dependent (Remorov et al., 2002;
 488 Mao et al., 2010; Cooper and Abbatt, 1996; Hanson et al., 1992; Thornton and Abbatt, 2005;
 489 Gershenzon et al., 1995). Here, RH and T were stabilized by the VACES–LFP–LIF system (in the
 490 reaction cell), as compared with those in ambient air (Fig. S8), statistical analysis indicates the RH and
 491 T in the reaction cell were on average decreased 3.3% (T-test, $p<0.05$, with inspection level = 0.05) and
 492 2.3 °C (T-test, $p<0.05$, with inspection level = 0.05), compared to that in ambient air, respectively,
 493 which is much smaller than the standard deviation of T and RH (which are ~3.7 °C and 16.4%, respectively)
 494 along with the measurement time. We noticed that k_a and γ showed no dependence on RH and T in the

495 reaction cell (see Fig. S9), indicating that the instantaneous change of RH and T may not be the
496 dominating factors in terms of the variation of k_a and γ with measurement time, and the stabilization of
497 RH and T by VACES–LFP–LIF system have negligible effects to k_a and γ . This suggests that the
498 individual chemical components and physical properties of ambient aerosols may dominate γ variation
499 during field campaign; both the metal-catalyzed reactions and the chemical components and their states
500 should be considered to yield more accurate γ values. Results obtained here are in accordance with
501 previous results on correlations between particulate H_2O_2 (which can be formed by the uptake of HO_2)
502 and coarse particulate transition metals (Wang et al., 2010). Using an offline methodology to investigate
503 the influence of RH and T by maintaining constant experimental conditions or chemical compositions
504 will be the subject of future work.

505 **3.5 Influence of the physical properties of ambient aerosols on k_a and γ**

506 HO_2 heterogeneous loss rates are driven by the different particle sizes of different aerosol types (i.e.,
507 urban ambient aerosols and marine aerosols)(Morita et al., 2004; Guo et al., 2019; Jacob, 2000). In this
508 study, k_a and γ showed no linear dependence on the mean ambient particle diameters (see Fig. S10).
509 Identifying the fractional contributions of aerosols in different particle size ranges to k_a and γ is highly
510 desirable in terms of understanding their influence. However, it seems that high γ values (> 0.8) occur
511 when the surface area is $< 2 \times 10^{-6} \text{ cm}^2 \text{ cm}^{-3}$ and the mean particle diameter is $< 110 \text{ nm}$. This is in
512 accordance with a previous study showing that aerosols yield the highest fractional contribution to the
513 total heterogeneous loss rate of HO_2 radicals of size $< 0.1 \text{ } \mu\text{m}$ (Morita et al., 2004) and that the mass
514 accommodation process plays the determining role for small and medium sized aerosols in controlling
515 HO_2 uptake. Guo et al. (2019) states the HO_2 radicals experience less loss upon its diffusion into larger
516 droplets than its diffusion into small droplets due to dilution effects make the larger aerosols having
517 lower depleting species concentrations (Cu^{2+}). However, this was based on the assumption that the total
518 mass of Cu^{2+} is constant during the hygroscopic growth of particles which is not always true in the
519 ambient conditions. Further studies about Cu^{2+} content in particles with different sizes are needed to
520 fully understand the result here.

521 **3.6 Significance of k_a to O_3 formation potential**

522 In urban atmosphere, XO_2 ($=\text{HO}_2+\text{RO}_2$) fate is important to the photochemical production of ozone
 523 ($\text{P}(\text{O}_3)$). Here, the loss rates of XO_2 due to three factors were compared: (i) uptake onto the ambient
 524 aerosols ($L_{\text{P}-\text{XO}_2}$ in Eq. 5), since no experiment or reference available for RO_2 uptake onto ambient
 525 particles, we assume the RO_2 reactivities caused by its interaction with ambient aerosols were the same
 526 as k_a , (ii) XO_2 self-reactions ($L_{\text{R}-\text{XO}_2}$ in Eq. 6), and (iii) reaction with NO ($L_{\text{N}-\text{XO}_2}$ in Eq. 7), which can
 527 produce NO_2 , a precursor of O_3 ; therefore Eq. 7 can also be regarded as $\text{P}(\text{O}_3)$.

528 $L_{\text{P}-\text{XO}_2} = k_a[\text{XO}_2]$ (5)

529 $L_{\text{R}-\text{XO}_2} = 2 * (k_{\text{HO}_2-\text{HO}_2}[\text{HO}_2]^2 + k_{\text{HO}_2-\text{RO}_2}[\text{HO}_2][\text{RO}_2])$ (6)

530 $L_{\text{NO}-\text{XO}_2} = k_{\text{NO}-\text{XO}_2}[\text{NO}][\text{XO}_2] = \text{P}(\text{O}_3)$ (7)

531 where $k_{\text{HO}_2-\text{HO}_2}$ and $k_{\text{HO}_2-\text{RO}_2}$ are the second-order rate constants of HO_2 self-reaction and its reaction
 532 with RO_2 , respectively. $k_{\text{NO}-\text{HO}_2}$ is the second-order rate constant of the reaction of HO_2 with NO . The
 533 HO_2 concentration was estimated from O_3 concentration using the method described by Kanaya et al.,
 534 (2007a). The RO_2 concentration is then estimated by assuming a steady state of HO_2 in the HO_x cycle;
 535 the reaction rates of HO_2 radicals are approximated as 0:

536
$$\frac{d[\text{HO}_2]}{dt} = P_{\text{HO}_2} - L_{\text{HO}_2} = k_{\text{CO-OH}}[\text{OH}][\text{CO}] + k_{\text{H}_2\text{CO-OH}}[\text{OH}][\text{H}_2\text{CO}] + k_{\text{NO-RO}_2}[\text{RO}_2][\text{NO}] -$$

 537
$$2k_{\text{HO}_2-\text{HO}_2}[\text{HO}_2][\text{HO}_2] - k_{\text{HO}_2-\text{RO}_2}[\text{HO}_2][\text{RO}_2] - k_{\text{NO-HO}_2}[\text{HO}_2][\text{NO}] - k_a[\text{HO}_2] = 0$$
 (8)

538 where $k_{\text{CO-OH}}$ and $k_{\text{H}_2\text{CO-OH}}$ are the second-order rate constants of the reactions of CO and H_2CO with
 539 OH , respectively. The different XO_2 loss rates described in Eqs. 5–7, along with the measurement times,
 540 are shown in Fig. 5a. Generally, $L_{\text{P}-\text{XO}_2}$ is much greater than $L_{\text{R}-\text{XO}_2}$, indicating that the XO_2 taken up
 541 by ambient aerosols will compete with the XO_2 self-reaction, thus influencing XO_2 concentration.
 542 However, such an influence may have a negligible impact on $\text{P}(\text{O}_3)$ because $L_{\text{P}-\text{XO}_2}$ is tens of thousands
 543 of times lower than $L_{\text{NO}-\text{XO}_2}$ owing to the relatively high NO_x concentration at Yokohama. We further
 544 tested the impact of $L_{\text{P}-\text{XO}_2}$ on ozone formation sensitivity regime, according to the method proposed
 545 by Sakamoto et al. (2019), in which L_N/Q is used as a new indicator:

546
$$\frac{\text{L}_N}{\text{Q}} = \frac{1}{1 + \left(\frac{(2k_{\text{R}}[\text{XO}_2] + k_a')k_{\text{OH-VOCS}}[\text{VOCS}]}{(1-\alpha')k_{\text{NO-HO}_2}[\text{NO}]k_{\text{OH-NO}_2}[\text{NO}_2]} \right)}$$
 (9)

547 where $k_{\text{OH-VOCs}}$ and $k_{\text{OH-NO}_2}$ are the second-order rate constants of the reactions of OH with VOCs
548 and NO_2 , respectively. $k_{\text{NO-HO}_2}$ is the second-order rate constant of the reaction of NO with HO_2 . α'
549 is the proportion of RO_2 in XO_2 . L_N is the OH radical loss rate through its reaction with NO_2 . ($=$
550 $k_{\text{OH-NO}_2}[\text{OH}][\text{NO}_2]$), and Q is the total loss of the HOx radicals in the HOx cycle reaction ($= L_N +$
551 $L_{\text{P-XO}_2} + L_{\text{R-XO}_2}$). The regime transition point can be expressed as

552
$$\frac{L_N}{Q_{\text{transition}}} = (1 - \chi) \frac{1}{2} + \chi \frac{1}{3} \quad (10)$$

553 where $\chi = L_{\text{P-XO}_2} / (L_{\text{P-XO}_2} + L_{\text{R-XO}_2})$. The results indicate that both L_N/Q and $L_N/Q_{\text{without_aerosol}}$
554 (calculated with and without including k_a' in Eq. 9, respectively) were higher than $L_N/Q_{\text{transition}}$,
555 indicating that ozone formation was VOC-sensitive throughout the campaign and that the aerosol uptake
556 of XO_2 (k_a') showed no impact on the O_3 formation regime (see Fig. 5, here we only consider the
557 daytime, when photochemical reactions occur). The plots of L_N/Q and $L_N/Q_{\text{without_aerosol}}$ as a
558 function of NO concentration show the values were closer to $L_N/Q_{\text{transition}}$ (~ 0.4) at lower NO
559 concentrations (Fig. S11); therefore, aerosol uptake may play a more important role in the O_3 formation
560 regime at NO levels lower than those observed in this study. The temporal variations in key factors used
561 in this section are shown in Fig. S12.

562

563

564

565

566

567

568

569

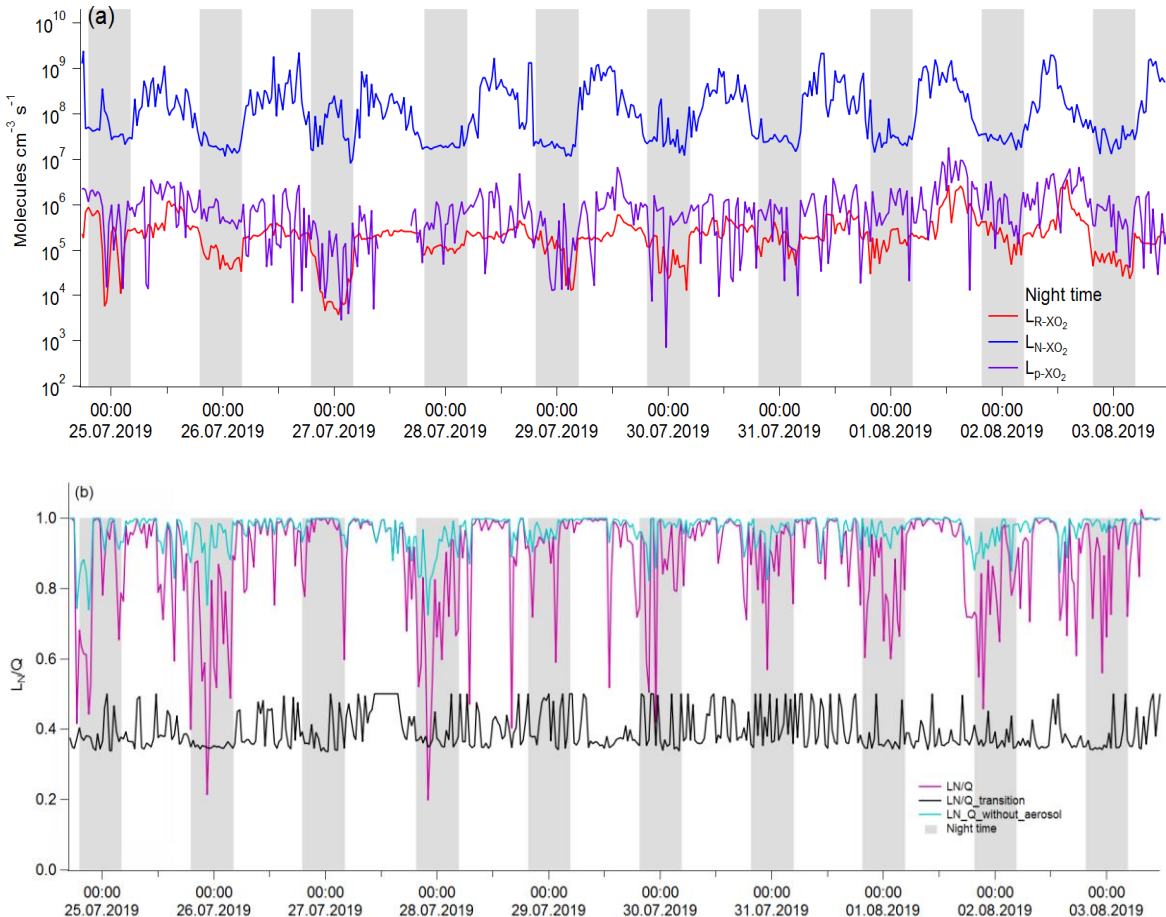


Figure 5: Temporal variations in (a) HO₂ radical loss rates and (b) L_N/Q (red line) and the regime transition threshold (L_N/Q_{transition}, black line) used to assess the ozone sensitivity regime. The gray shaded areas represent nighttime (from National Astronomical Observatory of Japan) and are not discussed herein.

4 Conclusions

This study used a reliable online methodology to investigate HO₂ uptake kinetics onto in situ ambient aerosols (i.e., HO₂ reactivity of ambient aerosols k_a and HO₂ uptake coefficients γ) and discussed the impacting factors on such processes, i.e., chemical compositions and physical properties of ambient aerosols and experimental conditions. k_a ranged between 0.001 s⁻¹ (25th percentile) and 0.005 s⁻¹ (75th percentile), with an average value of 0.005 ± 0.005 s⁻¹. The corresponding γ , ranged from 0.05 (25th percentile) to 0.33 (75th percentile), with the median value of 0.19 and the average value of 0.23 ± 0.21 , is comparable with previous measured (~0.24–0.25) (Zhou et al., 2019b; Taketani et al., 2012) and modeled (~0.20) values (Stadtler et al., 2018; Jacob, 2000). However, the k_a and γ values obtained here

595 are considered as the lower limit values for real ambient aerosols, as the coarse particles were not
596 measured in this study. We noticed that k_a and γ showed no dependence on RH and T in the reaction
597 cell in this study, indicating that the instantaneous change of RH and T may not be dominating factors
598 in terms of the variation of k_a and γ with measurement time, and the large standard deviation of the γ
599 values along with the measurement time (± 0.21 , 1σ) may be due to the instantaneously changed
600 chemical and physical properties of ambient aerosols, a large bias may exist if a constant γ value is used
601 for modeling.

602 We found that the individual chemical components of ambient aerosols may have collective effects
603 of to γ , through the analyses of 1) separating the air masses into two groups, group i from the ocean and
604 group ii from mainland Japan; 2) the average diurnal patterns; 3) the correlation matrix analysis of each
605 individual chemical component of ambient aerosol with k_a and γ ; and 4) the modeling studies using
606 previously proposed mechanisms. All these efforts clearly indicating that the transition metals contained
607 in ambient aerosols may act as a catalyst, thus accelerating the depletion of HO_2 , however, they can be
608 chelated by OA. OA can also cover the aerosol surface and alter the viscosity of ambient aerosols,
609 thereby decreasing γ , and that more oxidized organic aerosols tend to be highly viscous thus decrease
610 HO_2 uptake coefficients. Results obtained here are in accordance to previous laboratory and modeling
611 studies (Mao et al., 2013a; Lakey et al., 2016b; Lakey et al., 2016a; Takami et al., 2013; Thornton et al.,
612 2008; Hanson et al., 1994). The chemical components of ambient aerosols may be internally mixed, as
613 proposed by Takami et al. (2013), which influences the aerosol surface tension and the activity of the
614 free form of the copper ion (i.e., OA and BC) to constrain γ . In contrast to previous studies saying that
615 BC may shrink HO_2 losses onto ambient aerosols (Saathoff et al., 2001; Macintyre and Evans, 2011;
616 Bedjanian et al., 2005), we found BC positively correlated with HO_2 uptake coefficients (0.18), this
617 may be owing to BC can provide active sites or be coated by other chemical components thus facilitating
618 the physical uptake of HO_2 . Here, we observed higher γ values (> 0.8) when the mean particle diameter
619 is < 110 nm, identifying the fractional contributions of aerosols in different particle size ranges to k_a and
620 γ is highly desirable in terms of understanding their influence.

621 In summary, the chemical components and physical properties of ambient aerosols may dominate

622 γ variation during field campaign; to yield more accurate γ value, total suspended particles in ambient
623 air should be measured, and the metal-catalyzed reactions, chemical components, and aerosol states
624 should be considered. Also, improvements to the time-resolution of metal measurements are needed for
625 more precise analysis. For more detailed investigation of HO₂ uptake mechanisms, an offline
626 methodology that can maintain constant chemical compositions and experimental conditions (such as
627 RH and T) will be useful. The HO₂ loss onto ambient aerosols was identified to have a negligible impact
628 on the O₃ production rate and formation regime owing to the high NO_x concentrations at Yokohama.
629 This process may play a more important role in O₃ formation under low NO_x concentration and high
630 aerosol loading conditions. The results help us to understand the impacts of HO₂ uptake kinetics on
631 chemical transformations in troposphere.

632

633 Appendix:

634 Air mass directions (Figure S1), measurement strategy (Figure S2), a technique combined laser-flash
635 photolysis with laser-induced fluorescence (LFP-LIF), the enrichment of the ambient aerosols, HO₂
636 reactivity of ambient air, correction of gas-phase diffusion for HO₂ uptake coefficient, HO₂ reactivity
637 of ambient gas phase (k_g), examples of HO₂ decay profiles (Figure S3), HO₂ reactivity calibration with
638 different NO₂ concentrations (Figure S4), diurnal trends in individual chemical components of ambient
639 aerosols (Figure S5), diurnal trends in k_a and γ (Figure S6), correlations between measured and modeled
640 γ (Figure S7), time series of the averaged RH and T in ambient air and the reaction cell (Figure S8),
641 dependence of k_a and γ on RH in reaction cell (Figure S9), dependence of k_a and γ on mean particle
642 diameter (Figure S10), dependence of day time LN/Q and LN/Q_without_aerosol on [NO] (Figure
643 S11), profiles of key factors determining XO₂ loss rates and P(O₃) sensitivity (Figure S12), summary
644 of equations and values used for γ modeling (Table S1), summary of equations and values used for XO₂
645 (=HO₂+RO₂) loss and O₃ formation sensitivity regime (Table S1).

646

647 Author contribution

648 J.J., K.M., Y.S., and Y.K. designed the experiments and J.J. and Y.B. carried them out. J.J. did the data
649 analysis and prepared the manuscript with contributions from all co-authors.

650 Competing interests

651 The authors declare that they have no conflict of interest.

652 Data availability

653
654 Data supporting this publication are available upon request for the corresponding author
655 (junzhou@jnu.edu.cn).

656 Acknowledgments

657 This work was supported by the Japan Society for the Promotion of Science (JSPS) KAKENHI Grant
658 Numbers JP16H06305, JP19H04255. Many thanks to Yokohama Environmental Science Research
659 Institute utility during the campaign.

660 References

661 Baker, A. R., and Jickells, T. D.: Mineral particle size as a control on aerosol iron solubility, *Geophys.*
662 *Res. Lett.*, 33, 10.1029/2006GL026557, 2006.

663
664 Bertram, A. K., Martin, S. T., Hanna, S. J., Smith, M. L., Bodsworth, A., Chen, Q., Kuwata, M., Liu, A.,
665 You, Y., and Zorn, S. R.: Predicting the relative humidities of liquid-liquid phase separation,
666 efflorescence, and deliquescence of mixed particles of ammonium sulfate, organic material, and water
667 using the organic-to-sulfate mass ratio of the particle and the oxygen-to-carbon elemental ratio of the
668 organic component, *Atmos. Chem. Phys.*, 11, 10995–11006, 10.5194/acp-11-10995-2011, 2011.

669 Bedjanian, Y., Lelièvre, S., and Le Bras, G.: Experimental study of the interaction of HO₂ radicals with
670 soot surface, *Phys. Chem. Chem. Phys.*, 7, 334-341, 10.1039/B414217A, 2005.

671 Chen, G., Davis, D., Crawford, J., Heikes, B., O'Sullivan, D., Lee, M., Eisele, F., Mauldin, L., Tanner, D.,
672 Collins, J., Barrick, J., Anderson, B., Blake, D., Bradshaw, J., Sandholm, S., Carroll, M., Albercook, G.,
673 and Clarke, A.: An assessment of HO_x chemistry in the tropical pacific boundary layer: comparison of
674 model simulations with observations recorded during PEM Tropics A, *J. Atmos. Chem.*, 38, 317-344,
675 10.1023/A:1006402626288, 2001.

676
677 Cooper, P. L., and Abbatt, J. P. D.: Heterogeneous Interactions of OH and HO₂ Radicals with surfaces
678 characteristic of atmospheric particulate matter, *J. Phys. Chem.*, 100, 2249-2254, 10.1021/jp952142z,
679 1996.

680
681 DeCarlo, P. F., Kimmel, J. R., Trimborn, A., Northway, M. J., Jayne, J. T., Aiken, A. C., Gonin, M., Fuhrer,
682 K., Horvath, T., Docherty, K. S., Worsnop, D. R., and Jimenez, J. L.: Field-Deployable, High-Resolution,
683 Time-of-Flight Aerosol Mass Spectrometer, *Anal. Chem.* 78, 8281-8289, 10.1021/ac061249n, 2006.

684
685 Drinovec, L., Močnik, G., Zotter, P., Prévôt, A. S. H., Ruckstuhl, C., Coz, E., Rupakheti, M., Sciare, J.,
686 Müller, T., Wiedensohler, A., and Hansen, A. D. A.: The "dual-spot" Aethalometer: an improved
687 measurement of aerosol black carbon with real-time loading compensation, *Atmos. Meas. Tech.*, 8,
688 1965-1979, 10.5194/amt-8-1965-2015, 2015.
689
690 Fang, T., Guo, H., Zeng, L., Verma, V., Nenes, A., and Weber, R. J.: Highly acidic ambient particles,
691 soluble metals, and oxidative potential: a link between sulfate and aerosol toxicity, *Environ. Sci.
692 Technol.*, 51, 2611-2620, 10.1021/acs.est.6b06151, 2017.
693
694 Finlayson-Pitts, B. J., and Pitts, J. N.: CHAPTER 7 - Chemistry of inorganic nitrogen compounds, in:
695 chemistry of the upper and lower atmosphere, edited by: Finlayson-Pitts, B. J., and Pitts, J. N.,
696 Academic Press, San Diego, 264-293, 2000.
697
698 Fountoukis, C., and Nenes, A.: ISORROPIA II: a computationally efficient thermodynamic equilibrium
699 model for K^+ - Ca^{2+} - Mg^{2+} - NH_4^+ - Na^+ - SO_4^{2-} - NO_3^- - Cl^- - H_2O aerosols, *Atmos. Chem. Phys.*, 7, 4639-4659,
700 10.5194/acp-7-4639-2007, 2007.
701
702 George, I. J., and Abbatt, J. P.: Heterogeneous oxidation of atmospheric aerosol particles by gas-phase
703 radicals, *Nature chem.*, 2, 713-722, 10.1038/nchem.806, 2010.
704
705 George, I. J., Matthews, P. S. J., Whalley, L. K., Brooks, B., Goddard, A., Baeza-Romero, M. T., and Heard,
706 D. E.: Measurements of uptake coefficients for heterogeneous loss of HO_2 onto submicron inorganic
707 salt aerosols, *Phys. Chem. Chem. Phys.*, 15, 12829-12845, 10.1039/C3CP51831K, 2013.
708
709 Gershenzon, Y. M., Grigorieva, V. M., Ivanov, A. V., and Remorov, R. G.: O_3 and OH Sensitivity to
710 heterogeneous sinks of HO and CH_3O_2 on aerosol particles, *Faraday Discuss.*, 100, 83-100,
711 10.1039/FD9950000083, 1995.
712
713 George, C., Ammann, M., and Volkamer, R.: Heterogeneous photochemistry of imidazole-2-
714 carboxaldehyde: HO_2 radical formation and aerosol growth, *Atmos. Chem. Phys.*, 16, 11823-11836,
715 10.5194/acp-16-11823-2016, 2016.
716
717 Gonzalez, J., Torrent-Sucarrat, M., and Anglada, J. M.: The reactions of SO_3 with HO_2 radical and $H_2O\cdot\cdot$
718 HO_2 radical complex. Theoretical study on the atmospheric formation of HSO_5 and H_2SO_4 , *Phys. Chem.
719 Chem. Phys.*, 12, 2116-2125, 10.1039/B916659A, 2010.
720
721 González Palacios, L., Corral Arroyo, P., Aregahegn, K. Z., Steimer, S. S., Bartels-Rausch, T., Nozière, B.,
722 Guieu, C., Chester, R., Nimmo, M., Martin, J. M., Guerzoni, S., Nicolas, E., Mateu, J., and Keyse, S.:
723 Atmospheric input of dissolved and particulate metals to the northwestern Mediterranean, *Deep Sea
724 Res. (2 Top. Stud. Oceanogr.)*, 44, 655-674, 10.1016/S0967-0645(97)88508-6, 1997.
725
726 Guo, J., Tilgner, A., Yeung, C., Wang, Z., Louie, P. K. K., Luk, C. W. Y., Xu, Z., Yuan, C., Gao, Y., Poon, S.,
727 Herrmann, H., Lee, S., Lam, K. S., and Wang, T.: Atmospheric peroxides in a polluted subtropical
728 environment: seasonal variation, sources and sinks, and importance of heterogeneous processes,
729 *Environ. Sci. Technol.*, 48, 1443-1450, 10.1021/es403229x, 2014.
730
731 Guo, J., Wang, Z., Tao, W., and Zhang, X.: Theoretical evaluation of different factors affecting the HO_2
732 uptake coefficient driven by aqueous-phase first-order loss reaction, *Sci. Total Environ.*, 683, 146-153,
733 10.1016/j.scitotenv.2019.05.237, 2019.
734

735 Halstead, M. J. R., Cunningham, R. G., and Hunter, K. A.: Wet deposition of trace metals to a remote
736 site in Fiordland, New Zealand, *Atmos. Environ.*, 34, 665-676, 10.1016/S1352-2310(99)00185-5, 2000.
737

738 Hanson, D. R., Burkholder, J. B., Howard, C. J., and Ravishankara, A. R.: Measurement of hydroxyl and
739 hydroperoxy radical uptake coefficients on water and sulfuric acid surfaces, *J. Phys. Chem.*, 96, 4979-
740 4985, 10.1021/j100191a046, 1992.

741 Hanson, D. R., Ravishankara, A. R., and Solomon, S.: Heterogeneous reactions in sulfuric acid aerosols:
742 A framework for model calculations, *J. Geophys. Res. Atmos.*, 99, 3615-3629, 10.1029/93jd02932,
743 1994.

744

745 Heard, D. E., and Pilling, M. J.: Measurement of OH and HO₂ in the Troposphere, *Chem. Rev.*, 103,
746 5163-5198, 10.1021/cr020522s, 2003.

747

748 Hennigan, C. J., Izumi, J., Sullivan, A. P., Weber, R. J., and Nenes, A.: A critical evaluation of proxy
749 methods used to estimate the acidity of atmospheric particles, *Atmos. Chem. Phys.*, 15, 2775-2790,
750 10.5194/acp-15-2775-2015, 2015.

751

752 Hofmann, H., Hoffmann, P., and Lieser, K. H.: Transition metals in atmospheric aqueous samples,
753 analytical determination and speciation, *Fresen. J. Anal. Chem.*, 340, 591-597, 10.1007/BF00322435,
754 1991.

755

756 Hsu, S.-C., Wong, G. T. F., Gong, G.-C., Shiah, F.-K., Huang, Y.-T., Kao, S.-J., Tsai, F., Candice Lung, S.-C.,
757 Lin, F.-J., Lin, I. I., Hung, C.-C., and Tseng, C.-M.: Sources, solubility, and dry deposition of aerosol trace
758 elements over the East China Sea, *Mar. Chem.* 120, 116-127, 10.1016/j.marchem.2008.10.003, 2010.

759

760 J. Creasey, D., A. Halford-Maw, P., E. Heard, D., J. Pilling, M., and J. Whitaker, B.: Implementation and
761 initial deployment of a field instrument for measurement of OH and HO₂ in the troposphere by laser-
762 induced fluorescence, *J. Chem. Soc., Faraday Trans.* 93, 2907-2913, 10.1039/A701469D, 1997.

763

764 George, I. J., Slowik, J., and Abbatt, J.: Chemical aging of ambient organic aerosol from heterogeneous
765 reaction with hydroxyl radicals, *Geophys. Res. Lett.*, 35, L13811, 10.1029/2008GL033884, 2008.

766

767 Jacob, D. J.: Heterogeneous chemistry and tropospheric ozone, *Atmos. Environ.*, 34, 2131-2159,
768 10.1016/S1352-2310(99)00462-8, 2000.

769

770 Jaeglé, L., Jacob, D. J., Brune, W. H., Faloona, I., Tan, D., Heikes, B. G., Kondo, Y., Sachse, G. W.,
771 Anderson, B., Gregory, G. L., Singh, H. B., Pueschel, R., Ferry, G., Blake, D. R., and Shetter, R. E.:
772 Photochemistry of HO x in the upper troposphere at northern midlatitudes, *J. Geophys. Res. Atmos.*,
773 105, 3877-3892, doi:10.1029/1999JD901016, 2000.

774

775 Kanaya, Y., Cao, R., Akimoto, H., Fukuda, M., Komazaki, Y., Yokouchi, Y., Koike, M., Tanimoto, H.,
776 Takegawa, N., and Kondo, Y.: Urban photochemistry in central Tokyo: 1. Observed and modeled OH
777 and HO₂ radical concentrations during the winter and summer of 2004, *J. Geophys. Res. Atmos.*, 112,
778 10.1029/2007jd008670, 2007a.

779

780 Kanaya, Y., Cao, R., Kato, S., Miyakawa, Y., Kajii, Y., Tanimoto, H., Yokouchi, Y., Mochida, M., Kawamura,
781 K., and Akimoto, H.: Chemistry of OH and HO₂ radicals observed at Rishiri Island, Japan, in September
782 2003: Missing daytime sink of HO₂ and positive nighttime correlations with monoterpenes, 112,
783 10.1029/2006jd007987, 2007b.

784

785 Lakey, P. S. J., George, I. J., Whalley, L. K., Baeza-Romero, M. T., and Heard, D. E.: Measurements of
786 the HO₂ uptake coefficients onto single component organic aerosols, *Environ. Sci. Technol.*, 49, 4878-
787 4885, 10.1021/acs.est.5b00948, 2015.

788

789 Lakey, P. S. J., Berkemeier, T., Krapf, M., Dommen, J., Steimer, S. S., Whalley, L. K., Ingham, T., Baeza-
790 Romero, M. T., Pöschl, U., Shiraiwa, M., Ammann, M., and Heard, D. E.: The effect of viscosity and
791 diffusion on the HO₂ uptake by sucrose and secondary organic aerosol particles, *Atmos. Chem. Phys.*,
792 16, 13035-13047, 10.5194/acp-16-13035-2016, 2016a.

793

794 Lakey, P. S. J., George, I. J., Baeza-Romero, M. T., Whalley, L. K., and Heard, D. E.: Organics substantially
795 reduce HO₂ uptake onto aerosols containing transition metal ions, *J. Phys. Chem. A*, 120, 1421-1430,
796 10.1021/acs.jpca.5b06316, 2016b.

797

798 Logan, J. A., Prather, M. J., Wofsy, S. C., and McElroy, M. B.: Tropospheric chemistry: A global
799 perspective, 86, 7210-7254, 10.1029/JC086iC08p07210, 1981.

800

801 Loukhovitskaya, E., Bedjanian, Y., Morozov, I., and Le Bras, G.: Laboratory study of the interaction of
802 HO₂ radicals with the NaCl, NaBr, MgCl₂·6H₂O and sea salt surfaces, *Phys. Chem. Chem. Phys.*, 11,
803 7896-7905, 10.1039/B906300E, 2009.

804

805 Macintyre, H. L., and Evans, M. J.: Parameterisation and impact of aerosol uptake of HO₂ on a global
806 tropospheric model, *Atmos. Chem. Phys.*, 11, 10965-10974, 10.5194/acp-11-10965-2011, 2011.

807

808 Manoj, S. V., Mishra, C. D., Sharma, M., Rani, A., Jain, R., Bansal, S. P., and Gupta, K. S.: Iron, manganese
809 and copper concentrations in wet precipitations and kinetics of the oxidation of SO₂ in rain water at
810 two urban sites, Jaipur and Kota, in Western India, *Atmos. Environ.*, 34, 4479-4486, 10.1016/S1352-
811 2310(00)00117-5, 2000.

812

813 Mao, J., Jacob, D. J., Evans, M. J., Olson, J. R., Ren, X., Brune, W. H., Clair, J. M. S., Crounse, J. D., Spencer,
814 K. M., Beaver, M. R., Wennberg, P. O., Cubison, M. J., Jimenez, J. L., Fried, A., Weibring, P., Walega, J.
815 G., Hall, S. R., Weinheimer, A. J., Cohen, R. C., Chen, G., Crawford, J. H., McNaughton, C., Clarke, A. D.,
816 Jaeglé, L., Fisher, J. A., Yantosca, R. M., Le Sager, P., and Carouge, C.: Chemistry of hydrogen oxide
817 radicals (HO_x) in the Arctic troposphere in spring, *Atmos. Chem. Phys.*, 10, 5823-5838, 10.5194/acp-
818 10-5823-2010, 2010.

819

820 Mao, J., Fan, S., Jacob, D. J., and Travis, K. R.: Radical loss in the atmosphere from Cu-Fe redox coupling
821 in aerosols, *Atmos. Chem. Phys.*, 13, 509-519, 10.5194/acp-13-509-2013, 2013a.

822

823 Mao, J., Paulot, F., Jacob, D. J., Cohen, R. C., Crounse, J. D., Wennberg, P. O., Keller, C. A., Hudman, R.
824 C., Barkley, M. P., and Horowitz, L. W.: Ozone and organic nitrates over the eastern United States:
825 Sensitivity to isoprene chemistry, *J. Geophys. Res. Atmos.*, 118, 11,256-211,268, 10.1002/jgrd.50817,
826 2013b.

827

828 Martínez, M., Harder, H., Kovacs, T. A., Simpas, J. B., Bassis, J., Lesher, R. L., Brune, W., Frost, G.,
829 Williams, E., Stroud, C., Jobson, B., Roberts, J. M., Hall, S., Shetter, R., Wert, B. P., Fried, A., Aliche, B.,
830 Stutz, J., Young, V., White, A., and Zamora, R. J.: OH and HO₂ concentrations, sources, and loss rates
831 during the Southern Oxidants Study in Nashville, Tennessee, summer 1999, *J. Geophys. Res.*, 108, 2003.

832

833 Matthews, P. S. J., Baeza-Romero, M. T., Whalley, L. K., and Heard, D. E.: Uptake of HO₂ radicals onto
834 Arizona test dust particles using an aerosol flow tube, *Atmos. Chem. Phys.*, 14, 7397-7408,
835 10.5194/acp-14-7397-2014, 2014.

836
837 Millán, L., Wang, S., Livesey, N., Kinnison, D., Sagawa, H., and Kasai, Y.: Stratospheric and mesospheric
838 HO₂ observations from the Aura Microwave Limb Sounder, *Atmos. Chem. Phys.*, 15, 2889-2902,
839 10.5194/acp-15-2889-2015, 2015.
840 Miyazaki, K., Nakashima, Y., Schoemaecker, C., Fittschen, C., and Kajii, Y.: Note: A laser-flash photolysis
841 and laser-induced fluorescence detection technique for measuring total HO₂ reactivity in ambient air,
842 *Rev. Sci. Instrum.*, 84, 076106, 10.1063/1.4812634, 2013.
843
844 Morita, A., Kanaya, Y., and Francisco, J. S.: Uptake of the HO₂ radical by water: Molecular dynamics
845 calculations and their implications for atmospheric modeling, *J. Geophys. Res. Atmos.*, 109,
846 10.1029/2003jd004240, 2004.
847
848 Mozurkewich, M., McMurry, P. H., Gupta, A., and Calvert, J. G.: Mass accommodation coefficient for
849 HO₂ radicals on aqueous particles, *J. Geophys. Res. Atmos.*, 92, 4163-4170, 10.1029/JD092iD04p04163,
850 1987.
851
852 Nakayama, T., Matsumi, Y., Kawahito, K., Watabe, Y.: Development and evaluation of a palm-sized
853 optical PM_{2.5} sensor. *Aerosol Sci. Technol.*, 52, 2–12, 10.1080/02786826.2017.1375078, 2018.
854
855 Ng, N. L., Canagaratna, M. R., Jimenez, J. L., Chhabra, P. S., Seinfeld, J. H., and Worsnop, D. R.: Changes
856 in organic aerosol composition with aging inferred from aerosol mass spectra, *Atmos. Chem. Phys.*,
857 11, 6465-6474, 10.5194/acp-11-6465-2011, 2011.
858
859 Oakes, M., Weber, R. J., Lai, B., Russell, A., and Ingall, E. D.: Characterization of iron speciation in urban
860 and rural single particles using XANES spectroscopy and micro X-ray fluorescence measurements:
861 investigating the relationship between speciation and fractional iron solubility, *Atmos. Chem. Phys.*,
862 12, 745-756, 10.5194/acp-12-745-2012, 2012.
863
864 Remorov, R. G., Gershenzon, Y. M., Molina, L. T., and Molina, M. J.: Kinetics and mechanism of HO₂
865 uptake on solid NaCl, *J. Phys. Chem. A*, 106, 4558-4565, 10.1021/jp013179o, 2002.
866
867 Robinson, R. A., Stokes, R. H., and Marsh, K. N.: Activity coefficients in the ternary system: water +
868 sucrose + sodium chloride, *J. Chem. Thermodyn.*, 2, 745-750, 10.1016/0021-9614(70)90050-9, 1970.
869
870 Ross, H. B., and Noone, K. J.: A numerical investigation of the destruction of peroxy radical by Cu ion
871 catalysed reactions on atmospheric particles, *J. Atmos. Chem.*, 12, 121-136, 10.1007/BF00115775,
872 1991.
873
874 Saathoff, H., Naumann, K.-H., Riemer, N., Kamm, S., Möhler, O., Schurath, U., Vogel, H., and Vogel, B.:
875 The loss of NO₂, HNO₃, NO₃/N₂O₅, and HO₂/HOONO₂ on soot aerosol: A chamber and modeling study,
876 *Geophys. Res. Lett.*, 28, 1957-1960, 10.1029/2000gl012619, 2001.
877
878 Sadanaga, Y., Yoshino, A., Watanabe, K., Yoshioka, A., Wakazono, Y., Kanaya, Y., and Kajii, Y.:
879 Development of a measurement system of OH reactivity in the atmosphere by using a laser-induced
880 pump and probe technique, *Rev. Sci. Instrum.*, 75, 2648-2655, 10.1063/1.1775311, 2004.
881
882 Sakamoto, Y., Zhou, J., Kohno, N., Nakagawa, M., Hirokawa, J., and Kajii, Y.: Kinetics study of OH uptake
883 onto deliquesced NaCl particles by combining Laser Photolysis and Laser-Induced Fluorescence, *J. Phys.*
884 *Chem. Lett.*, 9, 4115-4119, 10.1021/acs.jpclett.8b01725, 2018.
885

886 Sakamoto, Y., Sadanaga, Y., Li, J., Matsuoka, K., Takemura, M., Fujii, T., Nakagawa, M., Kohno, N.,
887 Nakashima, Y., Sato, K., Nakayama, T., Kato, S., Takami, A., Yoshino, A., Murano, K., and Kajii, Y.:
888 Relative and absolute sensitivity analysis on ozone production in Tsukuba, a city in Japan, *Environ. Sci.*
889 *Technol.*, 53, 13629-13635, 10.1021/acs.est.9b03542, 2019.

890

891 Schwarz, J. P., Spackman, J. R., Fahey, D. W., Gao, R. S., Lohmann, U., Stier, P., Watts, L. A., Thomson,
892 D. S., Lack, D. A., Pfister, L., Mahoney, M. J., Baumgardner, D., Wilson, J. C., and Reeves, J. M.:
893 Coatings and their enhancement of black carbon light absorption in the tropical atmosphere, *J.*
894 *Geophys. Res. Atmos.*, 113, 10.1029/2007JD009042, 2008.

895 Sedlak, D. L., and Hoigné, J.: The role of copper and oxalate in the redox cycling of iron in
896 atmospheric waters, *Atmos. Environ.*, Part A. General Topics, 27, 2173-2185, 10.1016/0960-
897 1686(93)90047-3, 1993.

898 Siefert, R. L., Johansen, A. M., Hoffmann, M. R., and Pehkonen, S. O.: Measurements of trace metal
899 (Fe, Cu, Mn, Cr) oxidation states in fog and stratus clouds, *J. Air Waste Manage.*, 48, 128-143,
900 10.1080/10473289.1998.10463659, 1998.

901

902 Sioutas, C., Kim, S., Chang, M.: Development and evaluation of a prototype ultrafine particle
903 concentrator, *J. Aerosol Sci.* 30, 1001-1017, 10.1016/S0021-8502(98)00769-1, 1999.

904

905 Sommariva, R., Haggerstone, A. L., Carpenter, L. J., Carslaw, N., Creasey, D. J., Heard, D. E., Lee, J. D.,
906 Lewis, A. C., Pilling, M. J., and Zádor, J.: OH and HO₂ chemistry in clean marine air during SOAPEX-2,
907 *Atmos. Chem. Phys.*, 4, 839-856, 10.5194/acp-4-839-2004, 2004.

908

909 Song, H., Chen, X., Lu, K., Zou, Q., Tan, Z., Fuchs, H., Wiedensohler, A., Zheng, M., Wahner, A., Kiendler-
910 Scharr, A., and Zhang, Y.: Influence of aerosol copper on HO₂ uptake: A novel parameterized equation,
911 *Atmos. Chem. Phys. Discuss.*, 2020, 1-23, 10.5194/acp-2020-218, 2020.

912

913 Stadtler, S., Simpson, D., Schröder, S., Taraborrelli, D., Bott, A., and Schultz, M.: Ozone impacts of gas-
914 aerosol uptake in global chemistry transport models, *Atmos. Chem. Phys.*, 18, 3147-3171,
915 10.5194/acp-18-3147-2018, 2018.

916

917 Stone, D., Whalley, L. K., and Heard, D. E.: Tropospheric OH and HO₂ radicals: field measurements and
918 model comparisons, *Chem. Soc. Rev.*, 41, 6348-6404, 10.1039/C2CS35140D, 2012.

919

920 Takami, A., Mayama, N., Sakamoto, T., Ohishi, K., Irei, S., Yoshino, A., Hatakeyama, S., Murano, K.,
921 Sadanaga, Y., Bandow, H., Misawa, K., and Fujii, M.: Structural analysis of aerosol particles by
922 microscopic observation using a time-of-flight secondary ion mass spectrometer, *J. Geophys. Res.*
923 *Atmos.*, 118, 6726-6737, 10.1002/jgrd.50477, 2013.

924

925 Taketani, F., Kanaya, Y., and Akimoto, H.: Kinetics of heterogeneous reactions of HO₂ radical at
926 ambient concentration levels with (NH₄)₂SO₄ and NaCl aerosol particles, *J. Phys. chem. A*, 112, 2370-
927 2377, 10.1021/jp0769936, 2008.

928

929 Taketani, F.; Kanaya, Y.; Akimoto, H., Heterogeneous loss of HO₂ by KCl, synthetic sea salt, and natural
930 seawater aerosol particles. *Atmos. Environ.*, **2009**, 43, (9), 1660-1665.

931

932 Taketani, F., Kanaya, Y., Pochanart, P., Liu, Y., Li, J., Okuzawa, K., Kawamura, K., Wang, Z., and Akimoto,
933 H.: Measurement of overall uptake coefficients for HO₂ radicals by aerosol particles sampled from
934 ambient air at Mts. Tai and Mang (China), *Atmos. Chem. Phys.*, 12, 11907-11916, 10.5194/acp-12-
935 11907-2012, 2012.

936 Thornton, J., and Abbatt, J. P. D.: Measurements of HO₂ uptake to aqueous aerosol: Mass
937 accommodation coefficients and net reactive loss, *J. Geophys. Res. Atmos.*, 110,
938 10.1029/2004jd005402, 2005.

939

940 Thornton, J. A., Jaeglé, L., and McNeill, V. F.: Assessing known pathways for HO₂ loss in aqueous
941 atmospheric aerosols: Regional and global impacts on tropospheric oxidants, *J. Geophys. Res. Atmos.*,
942 113, 10.1029/2007jd009236, 2008.

943

944 Tie, X., Brasseur, G., Emmons, L., Horowitz, L., and Kinnison, D.: Effects of aerosols on tropospheric
945 oxidants: A global model study, *J. Geophys. Res. Atmos.*, 106, 22931-22964, 10.1029/2001JD900206,
946 2001.

947

948 Wang, Y., Arellanes, C., Curtis, D. B., and Paulson, S. E.: Probing the source of hydrogen peroxide
949 associated with coarse mode aerosol particles in southern California, *Environ. Sci. Technol.*, 44, 4070-
950 4075, 10.1021/es100593k, 2010.

951

952 Wang, D., Pakbin, P., Saffari, A., Shafer, M. M., Schauer, J. J., and Sioutas, C.: Development and
953 evaluation of a high-volume aerosol-into-liquid collector for fine and ultrafine particulate matter,
954 *Aerosol Sci. Technol.*, 47, 1226-1238, 10.1080/02786826.2013.830693, 2013.

955

956 Wang, D., Shafer, M. M., Schauer, J. J., and Sioutas, C.: Development of a technology for online
957 measurement of total and water-soluble copper (Cu) in PM_{2.5}, *Aerosol Sci. Technol.*, 48, 864-874,
958 10.1080/02786826.2014.937478, 2014.

959 Whalley, L. K., Furneaux, K. L., Goddard, A., Lee, J. D., Mahajan, A., Oetjen, H., Read, K. A., Kaaden, N.,
960 Carpenter, L. J., Lewis, A. C., Plane, J. M. C., Saltzman, E. S., Wiedensohler, A., and Heard, D. E.: The
961 chemistry of OH and HO₂ radicals in the boundary layer over the tropical Atlantic Ocean, *Atmos. Chem.
962 Phys.*, 10, 1555-1576, 10.5194/acp-10-1555-2010, 2010.

963

964 Wilkinson, J., Reynolds, B., Neal, C., Hill, S., Neal, M., and Harrow, M.: Major, minor and trace element
965 composition of cloudwater and rainwater at Plynlimon, *Hydrol. Earth Syst. Sci.*, 1, 557-569,
966 10.5194/hess-1-557-1997, 1997.

967

968 You, Y., Smith, M. L., Song, M., Martin, S. T., and Bertram, A. K.: Liquid-liquid phase separation in
969 atmospherically relevant particles consisting of organic species and inorganic salts, *Int. Rev. Phys.
970 Chem.*, 33, 43-77, 10.1080/0144235X.2014.890786, 2014.

971 Zhou, J., Elser, M., Huang, R. J., Krapf, M., Fröhlich, R., Bhattu, D., Stefenelli, G., Zotter, P., Bruns, E. A.,
972 Pieber, S. M., Ni, H., Wang, Q., Wang, Y., Zhou, Y., Chen, C., Xiao, M., Slowik, J. G., Brown, S., Cassagnes,
973 L. E., Daellenbach, K. R., Nussbaumer, T., Geiser, M., Prévôt, A. S. H., El-Haddad, I., Cao, J.,
974 Baltensperger, U., and Dommen, J.: Predominance of secondary organic aerosol to particle-bound
975 reactive oxygen species activity in fine ambient aerosol, *Atmos. Chem. Phys.*, 19, 14703-14720,
976 10.5194/acp-19-14703-2019, 2019a.

977 Zhou, J., Murano, K., Kohno, N., Sakamoto, Y., and Kajii, Y.: Real-time quantification of the total HO₂
978 reactivity of ambient air and HO₂ uptake kinetics onto ambient aerosols in Kyoto (Japan), *Atmosp.
979 Environ.*, 117189, 10.1016/j.atmosenv.2019.117189, 2019b.

980